ETH
Eidgenössische Technische Hochschule Zürich
Swiss Federal Institute of Technology Zurich

Institute for
Dynamic Systems and Control
IDSC
Institut für Dynamische Systeme
und Regelungstechnik

Tobias Sutter

A Dynamical Approach to Create Different Juggling Patterns Using Chaos

Bachelor Thesis

Institute for Dynamic Systems and Control
Swiss Federal Institute of Technology (ETH) Zurich

Supervision

Philipp Reist
Prof. Dr. Raffaello D'Andrea

June 2010

Preface

During the last four months, I had the chance to write my Bachelor thesis at the Mechanical Engineering Departement of the ETH Zurich. First at all, I would like to express my gratitude to Phlilipp Reist for his enthusiasm, never ending patience and availability in excellent scientific supervision. His vast experience in nonlinear dynamics has greatly helped me understand the matter. Several parts, as the perturbation analysis, would not have been possible without him. In addition, I would like to thank him for coming up with the fascinating task.

Furthermore, I thank Professor Raffaello D'Andrea for his valuable comments and for giving me the opportunity to write this thesis at the Institute for Dynamic Systems and Control of the ETH Zurich. Last but not least, I sincerely thank PD. Dr. Remco I. Leine and Thomas F. Heimsch for the fruitful discussions.

This thesis has not only helped me gain insight into the captivating area of nonlinear dynamics, but also showed me how to conduct scientific research.

Contents

Abstract

A bouncing ball on a vibrating plate is a canonical example of a dynamic system, exhibiting nonlinear phenomena, such as chaos and it is easy to study experimentally. We present two strategies to create different juggling patterns for a blind juggling robot that juggles four balls at the same time. An algorithm to realize four desired periodic orbits is introduced starting with four balls in the $\mathcal{P}_1^1$-orbit, where the paddle's trajectory is used as control input. The key idea is to use two different paddle modes and to switch it at an appropriate time. The first mode has the goal to 'break the symmetry' of the four balls, i.e. we separate their trajectories from each other. This is done by a paddle trajectory that produces chaotic motion of the balls. Then, suitable ball's states have to be induced such that the paddle's trajectory can be switched to the second mode and the desired combination of four periodic orbits results. As a basic requirement for this approach we need to know what suitable ball's states are. Therefore, the basin of attraction for each periodic orbit is determined by numerical simulation. Using the basin of attraction, each ball's state at a potential switching point can be classified whether it leads to the desired periodic orbit or not.

Notation

The following notations and abbreviations are standard and used throughout the text. Other non-standard notations are defined when first introduced.

Sets

$a \in A$	a is an element of the set A
$[a, b]$	the closed interval $\{x \in \mathbb{R} \vert a \leq x \leq b\}$
(a, b)	the open interval $\{x \in \mathbb{R} \vert a < x < b\}$
$\{a, b\}$	the set comprising the elements {a} and {b}
$A \cup B$	union of set A and B

Algebra

$\mathbb{R}$	set of real numbers
$\mathbb{R}_+$	set of non-negative real numbers
$\mathbb{Z}$	set of integer numbers
$\mathbb{N}$	set of natural numbers
A^n	set of n-tuples of elements belonging to the set A (e.g. $\mathbb{R}^n$)
x	scalar
$\mathbf{x}$	vector in $\mathbb{R}^2$
$\mathbf{x}_i$	i$^{\text{th}}$ element of $\mathbf{x}$

Analysis

$\vert x \vert$	absolute value of x
$\Vert \mathbf{x} \Vert$	Euclidian norm of a vector
$\Vert \mathbf{x} \Vert_\infty$	infinity norm of a vector
$a := b$	a is defined by b

Acronyms and Abbreviations

BJR	Blind Juggling Robot
NNA	Nearest Neighbour Algorithm
WAA	Weighted Average Algorithm
CA	Connectivity Algorithm
RA	Robust Algorithm

Chapter 1

Introduction

1.1 Motivation

Today's science is interdisciplinary. One highly interdisciplinary field is nonlinear dynamics, which has wide applications in engineering, mathematics, biology and physics - to only list a limited number. These fields are united by the fact that models to describe some phenomena are derived, which is often done using nonlinear equations. The handling of such models motivated scientists as Euler, Lagrange, Hamilton and Maxwell to analyze the nonlinear dynamics of such systems. According to [1], Heri Poincaré (1892) was the first that discovered one of the main characteristics that arise in nonlinear systems - the sensitive dependence on initial conditions - which is a major characteristic of a chaotic system. Illustrating the mentioned interdisciplinarity, it was a meteorologist called E.N. Lorenz (1963), that discovered a second characteristic of chaotic systems - the fact that solutions never settle down to equilibrium or to a periodic state (aperiodic long-term behaviour). This was done by computer simulation, which already indicates that nonlinear systems can be rather hard to handle analytically.

The motion of a bouncing ball is perhaps one of the simplest physical system which shows the characteristics of a chaotic system mentioned above. Futhermore, it is easy to experimentally study the dynamics of a bouncing ball system. The bouncing ball system is a hybrid dynamical system, where flows are described by differential equations and impacts by difference equations. Again, the bouncing ball sytem is a canonical example of a hybrid system.
Due to the fact of being a comprehensible example representing the phenomena mentioned above, the bouncing ball system has been extensively studied by dynamical systems theorists. However, the bouncing ball system appears in many different applied fields, as the control and noise generation of machinery such as jackhammers, the transportation and separation of granular solids such as rice, or hopping robots.

According to [2], the stabilization of a ball juggling system to rhythmic patterns - as an extension of the bouncing ball system - has received great attention from the engineering and neuroscience community because of its relevance in robotics and nature. The problem that is adressed in this thesis (see Section 1.4) is highly interesting because it unites everything mentioned before.

1.2 Literature Survey

Because of its completeness in exhibiting the nonlinear phenomena mentioned in Section 1.1 and due to its practical relevance, juggling systems have been widely studied. According to [3], Bühler, Koditschek and Kindlmann [4] were amongst the first analyzing a juggling robot. Using a feedback algorithm called 'mirror algorithm', they were able to bring a ball to a desired periodic orbit.
In [3], Reist presented a new strategy of stabilizing the ball by an appropriate paddle curvature without using any knowledge about the ball's state at any time. He showed that the closed loop performance is only marginally better than what is achieved with open loop control. His blind juggling robot (BJR), presented in [3], is used as reference with regard to later implement the strategy derived in this thesis. Therefore, all physical limitations of the BJR are taken into account within this thesis.
Recently, Sanfelice, Teel and Sepulchre [2] presented a control stragety for a one degree-of-freedom juggling robot, that - with only the information of the ball's state at impacts - controls the ball to track a reference rhythmic pattern. Their main idea is to optimize the paddle trajectory after each impact such that a reference trajectory is tracked. Furhtermore, a modeling of the bouncing ball as hybrid dynamical system, as mentioned in Section 1.1, is given. They close with an extension of their 'hybrid control stragegy' to juggle multiple balls with different rhythmic patterns.

The two approaches presented in [5] and [6] share the idea to compute the basin of attraction for a desired periodic orbit. This is done by linearizing the bouncing ball system about an equilibrium point and then compute numerically a Lyapunov function for the linearized system. In this way, a basin of attraction for the nonlinear system in some neighbourhood of the reference solution is obtained - in other words, a local stability estimation is performed. Vincent [6] illustrates a challenging approach that highly influenced this thesis: He uses a paddle trajectory producing chaotic motion of the ball to enter the basin of attraction, that is precomputed and therefore known and then switches the paddle frequency to reach a particular periodic orbit. Summing up, he reduces the problem of stabilizing a ball juggling in a certain periodic orbit, to the computation of its basin of attraction together with the task to find a suitable excitation such that this basin of attraction can be reached.

In literature, juggling robots or more general bouncing ball systems are mostly analyzed for sinusoidally vibrating paddles, as in [1],[5],[6],[7] and [8]. With respect to the BJR, where the paddle is driven by a servo controller that is limited to quadratic trajectories, we cannot choose a sinusoidal paddle trajectory. Instead, a piecewise parabolic paddle trajectory, developed in [3], is used. However, this piecewise trajectory highly complicates the analysis of the bouncing ball system, since - in contrast to a sinusoidal trajectory - a case distinction has to be introduced. Therefore, we consider a numerical approach in this thesis. In chapter 4, we focus only on one parabolic piece of the paddle trajectory, which simplifies the analysis and would make an analytic stability treatment, similar to [7], possible.

1.3 Purpose

In this section, the main goal of this thesis is introduced. Using the BJR presented in [3], several periodic orbits can be reached. However, the initial condition, i.e. the initial height of the ball, where it is dropped, has to be laboriously generated by hand. Therefore, it is already hard to reach a periodic orbit and in case a periodic orbit is reached, it is most likely the 'one periodic' orbit, where the ball hits at each paddle period. We use a paddle as presented in Fig. 1.1 to juggle four balls at the same time. Hence, different periodic orbits can be realized by different balls, which characterizes a certain juggling pattern of the whole system.

One can easily start this paddle from rest such that all four balls reach the mentioned 'one periodic' orbit. The task of this thesis was to come up with a strategy to realize different juggling patterns, i.e. different combinations of periodic orbits, while starting with all four balls in the 'one periodic' orbit. A possible juggling pattern can be seen in Fig. 1.1. To realize a desired pattern, firstly we have to break the symmetries - in other words we have to somehow separate the balls from each other. In a second step, when the four balls have different trajectories, we want them to reach the four desired periodic orbits.

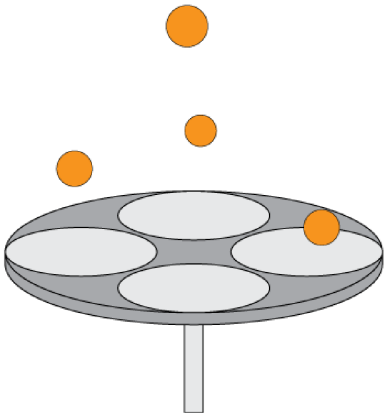

Figure 1.1: Cloverleaf paddle with an exemplary juggling pattern

1.4 Thesis Outline

Chapter 2 describes how the system is modeled and what fundamental assumptions it is based on. After having introduced some basic notation and concepts, as the Newton's impact law, the system of differential equations - describing the ball's flight between two impacts - and the so-called impact map (difference equation), which relates two pre-impact states, is derived. Furthermore, the two different modes of the paddle trajectory are presented leading to the total number of different periodic orbits that are feasible by the BJR.

Chapter 3 is concerned with the derivation of an algorithm to fulfill the task given in Section 1.3. The basins of attraction for the feasible periodic orbits are computed, which are major components of the algorithm. As it is done numerically by discretizing the state space, one needs a method to classify a point, which does not

exactly fit one of the computed grid points - as most of the measured data points will not do. Therefore, four interpolation algorithms are derived and compared related to performance. Subsequently, a paddle trajectory, similar to [6], is derived such that the ball states enter a desired basin of attraction. We present multiple reasons, why the paddle trajectory is chosen such that chaotic motion is produced. The algorithm, which is - to keep it as simple as possible - firstly derived for one ball, is then extended to handle multiple balls.

Chapter 4 is dedicated to a second algorithm that fulfills the given task. Another approach is considered where the main drawbacks of the first strategy should be improved. Namely, the low robustness and the waiting times. Nevertheless, some results derived in chapter 3 are absorbed. Furthermore, a local stability analysis is given.

The final chapter draws some conclusions and possible future work is proposed.

Chapter 2

The Bouncing Ball Model

In this chapter, a model for the bouncing ball system is derived, which has been - as already mentioned - extensivly studied. However, the underlying assumptions vary from a 'high bounce approximation' and elastic impact, as in [1], to a negligible effect of the ball's collision to the paddle trajecotry, in [1],[5],[7],[8]. Whereas in [2], the fewest assumptions are used which leads to a more complex system modelling. In order to focus on the given task, reasonable assumptions have to be made. We have to compromise about physical accuracy and mathematical simplicity of the model. Therefore, we consider a ball in a constant gravitational field and model the impacts of the ball and paddle as an inelastic collision, i.e. there is energy dissipation which is described by the coefficient of restitution. Furthermore, the paddle's mass is assumed to be much greater than the ball's mass so that the ball's impact contribution to the paddle trajectory is negligible. This assumption is clearly justified by the real BJR, where the ball's mass is roughly 3×10^{-4} times smaller than the paddle's mass, according to [3]. Since only the vertical motion is considered, the system has one degree-of-freedom. Again, this assumption is reasonable, as in [3] horizonal stability for the BJR is proved up to a certain apex height.

2.1 Impact Map and State Relation

The dynamics of a ball bouncing on an actuated racket are hybrid, as mentioned in Section 1.1. Between two impacts, the ball follows a parabolic trajecotry, plotted in Fig. 2.2. To describe the ball's trajectory we choose the ball's state as

$$\mathbf{x_B}(t) := \begin{pmatrix} x_B(t) \\ \dot{x}_B(t) \end{pmatrix} \tag{2.1}$$

and describe the free flight as a system of ordinary differential equations

$$\dot{\mathbf{x}}_\mathbf{B}(t) = \frac{d}{dt} \begin{pmatrix} x_B(t) \\ \dot{x}_B(t) \end{pmatrix} = \begin{pmatrix} \dot{x}_B(t) \\ -g \end{pmatrix} \tag{2.2}$$

with initial conditions

$$\mathbf{x_B}(0) = \begin{pmatrix} x_B(0) \\ \dot{x}_B(0) \end{pmatrix}. \tag{2.3}$$

The solution of (2.2), which is derived using standard methods,

$$\begin{pmatrix} x_B(t) \\ \dot{x}_B(t) \end{pmatrix} = \begin{pmatrix} -\frac{1}{2}gt^2 + \dot{x}_B(0)t + x_B(0) \\ -gt + \dot{x}_B(0) \end{pmatrix} \tag{2.4}$$

describes the ball dynamics between two impacts. Choosing the initial condition $x_B(0) = 0$ leads to

$$t = \frac{1}{g}(\dot{x}_B(0) - \dot{x}_B(t)). \tag{2.5}$$

Inserting (2.5) in (2.2) results in

$$\dot{x}_B^2(t) = -2gx_B(t) + \dot{x}_B^2(0). \tag{2.6}$$

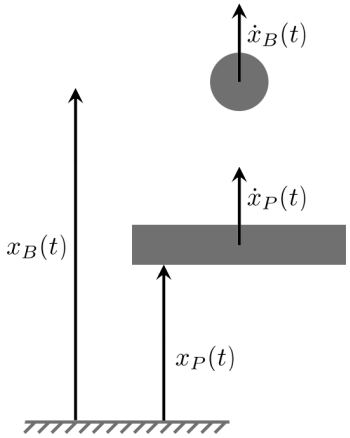

Figure 2.1: The bouncing ball system

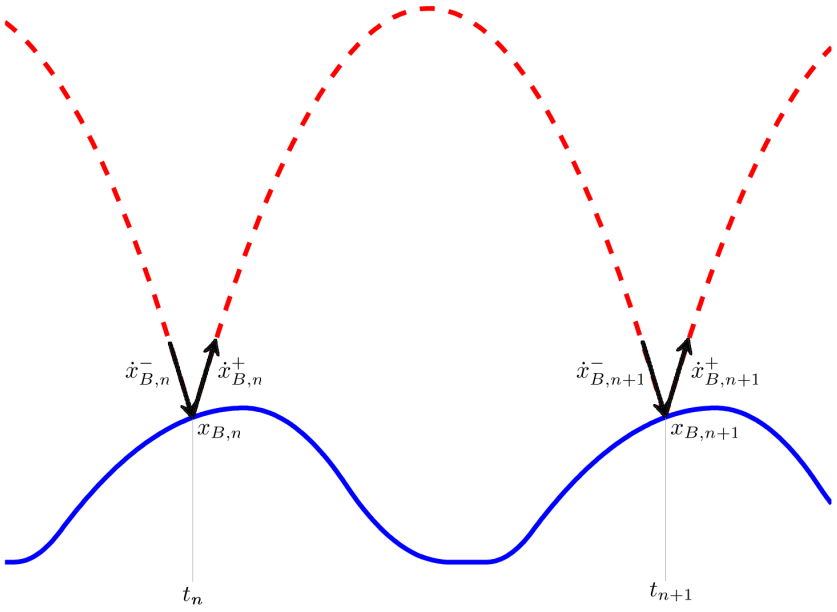

Figure 2.2: Notation for the discretization

The positions where the impacts occur are described by a discrete time system. Let $x_{B,n}$ be the position of the n$^{\text{th}}$-impact, $\dot{x}^-_{B,n}$ and $\dot{x}^+_{B,n}$ the velocitiy of the ball immediately before(-) and immediately after(+) the n$^{\text{th}}$-impact, according to

Fig. 2.2 We assume the impact to occur instantaneously, i.e. $x^-_{B,n} = x^+_{B,n}$ and $x^-_{P,n} = x^+_{P,n}$, where

$$\mathbf{x_P}(t) := \begin{pmatrix} x_P(t) \\ \dot{x}_P(t) \end{pmatrix} \tag{2.7}$$

is the paddle's state. Since the collisions are assumed to be inelastic, there is an energy dissipation at each impact described by the coefficient of restitution e_z, where $e_z \in [0, 1]$. The limiting value $e_z = 1$ characterizes the elastic collision, i.e. the ideal case with no energy dissipation, whereas for $e_z = 0$ the ball immediately lies on the surface with which it collides. Within few steps a mapping between pre- and post-impact states can be derived. This is done in [1] and is known as Newton's impact law

$$\dot{x}^+_{B,n} = -e_z \dot{x}^-_{B,n} + (1 + e_z)\dot{x}_{P,n}. \tag{2.8}$$

Now, the discrete time system of the impact states can be derived using (2.6) and the variables defined according to Fig. 2.2. We define the time between two impacts as

$$\Delta t_n := t_{n+1} - t_n. \tag{2.9}$$

By using the initial condition $\mathbf{x_B}(\mathbf{0}) := \mathbf{x^+_{B,n}}$, we can describe the impact state after the fee flight as

$$x_{B,n+1} = x_{P,n+1} = x_P(\Delta t_n) \tag{2.10}$$

$$\dot{x}^-_{B,n+1} = -\sqrt{\left(\dot{x}^+_{B,n}\right)^2 - 2g(x_{B,n+1} - x_{B,n})}. \tag{2.11}$$

To determine the time Δt_n up to the next impact, (2.8) is placed into (2.4) which leads to

$$x_{B,n+1} = -\frac{1}{2}g(\Delta t_n)^2 + \left(-e_z \dot{x}^-_{B,n} + (1 + e_z)\dot{x}_{P,n}\right)\Delta t_n + x_{B,n}. \tag{2.12}$$

Having derived all the required equations, a formulation for the discrete time system of the impact states can be given as

$$\begin{aligned} x_{B,n+1} &= x_P(\Delta t_n) \\ \dot{x}^-_{B,n+1} &= -\sqrt{\left((1 + e_z)\dot{x}_{P,n} - e_z \dot{x}^-_{B,n}\right)^2 - 2g(x_{B,n+1} - x_{B,n})} \end{aligned}$$

where Δt_n results from

$$-\frac{1}{2}g(\Delta t_n)^2 + \left(-e_z \dot{x}^-_{B,n} + (1 + e_z)\dot{x}_{P,n}\right)\Delta t_n - (x_{B,n+1} - x_{B,n}) = 0, \tag{2.13}$$

which is called the impact map and is equivalent to the formulation in [5]. The two equations (2.4) and (2.13) fully characterize the nonlinear dynamics of the bouncing ball system. According to [5] the impact map is transcendental and cannot be solved analytically. However, we can approximate it numerically and use it for the simulations that are performed in Chapter 3. It could be solved analytically by assuming that the impacts always occur at the same paddle position ('high bounce approximation', according to [1]). After [5], stable cycles manifest themselves in fixed points of (2.13).

2.2 Paddle Trajectory

The paddle movement is assumed as a periodic trajectory that is known. Without any doubt a non periodic paddle trajectory has several advantages, that are pointed out in [2]. However, to keep it as simple as possible, we choose the paddle trajectory as periodic. There are two different types of trajectories: The stabilizing trajectory where the stability analysis is based on and the so-called chaos trajecotry which is used to excite the ball and generate an appropriate ball state. The parameters of each trajectory were selected under several criterions, as described in Section 2.2.3.

2.2.1 Stabilizing Paddle Trajectory

As shown in [5], stability of the apex height can be achieved by choosing the paddle acceleration a_p at the impact smaller than zero and in a certain range. The BJR consists of a linear motor which actuates the paddle. Therefore, according to [3], the paddle's trajectory has to be chosen piecewise quadratic. Since the parameters of the paddle trajectory have already been optimized in [3], it could simply be reproduced. As shown in Fig. 2.3, the paddle curve consists of five parabolic parts. For the stability analysis in Chapter 4 only the second part of the curve, where the nominal impact point is located, will be considered.

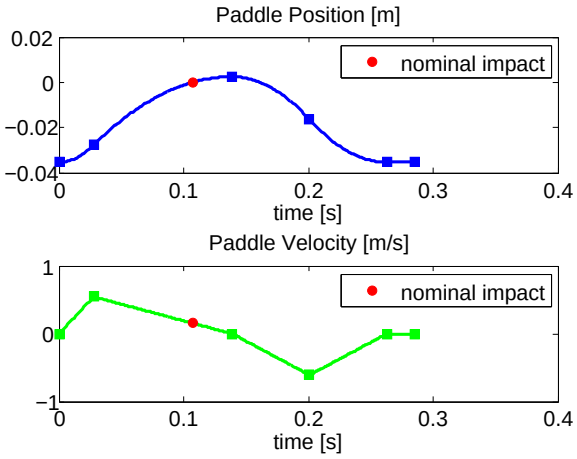

Figure 2.3: Stabilizing paddle trajectory

2.2.2 Chaos Paddle Trajectory

As explained in Chapter 1, before switching back to the stabilizing paddle curve, an extensive set of initial conditions for the ball has to be induced. This is realized by a paddle trajectory that produces chaotic behavior of the balls. Why the paddle curve in Fig. 2.4 produces chaos and what we exactly denote with chaos is explained in Section 3.3 in more detail. Nevertheless, the formal implementation of the paddle excitation is given here. The chaos paddle curve

$$x_p(t) = \begin{cases} -\frac{1}{2}a_c t^2 + v_0 t, & \text{if } t \in [kT_c, (k+\frac{1}{2})T_c], k \in \mathbb{Z} \\ \frac{1}{2}a_c t^2 - v_0 t, & \text{if } t \in [(k+\frac{1}{2})T_c, (k+1)T_c,], k \in \mathbb{Z} \end{cases} \tag{2.14}$$

is assembled from two parabolic pieces with relatively high frequency. It is fully characterized through the selection of the maximum stroke A and the paddle's acceleration a_c. To compute the maximum stroke, the maximum of (2.14) is derived:

$$\dot{x}_P(t) = -a_c t + v_0 \stackrel{!}{=} 0 \quad \Rightarrow \quad t_m := \frac{v_0}{a_c} \tag{2.15}$$

$$\underbrace{x_p(t_m)}_{A} = \frac{1}{2}\frac{v_0^2}{a_c} \quad \Rightarrow \quad v_0 = \sqrt{2Aa_c} \tag{2.16}$$

The period of the chaos trajectory T_c can be derived by comparing the velocities of both parts.

$$v_0 = a_c\frac{1}{2}T_c - v_0 \quad \Rightarrow \quad T_c = \sqrt{\frac{32A}{a_c}} \tag{2.17}$$

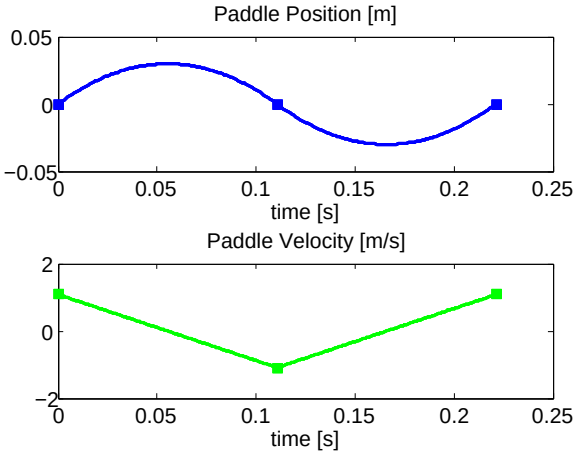

Figure 2.4: Chaos paddle trajectory

2.2.3 Parameters

Before we continue with the analysis, an overview about the used parameters is given in Tab. 2.1. The experimental value for the coefficient of restitution was derived in [9]. However, it could be changed varying the balls by using different materials. The determination of the characteristic parameters a_c and T_c for the chaos paddle trajectory is described in Section 3.3. Finally, the stabilizing paddle acceleration refers to the piece in Fig. 2.3, that contains the nominal impact point. The according value was derived in [3].

Table 2.1: Reference values for the bouncing ball system

Parameter	Symbol	Experimental Value
Gravitational acceleration	g	9.81 $\frac{m}{s^2}$
Coefficient of restitution	e_z	0.8
Chaos paddle acceleration	a_c	$\pm 2g$
Chaos maximum stroke	A	0.03 m
Chaos paddle period	T_c	0.2212 s
Chaos maximum velocity	v_0	1.0850 $\frac{m}{s^2}$
Stabilizing paddle acceleration	a_p	$-\frac{1}{2}g$

2.3 Feasibility of Periodic Orbits

As mentioned in Section 1.3 the goal of this thesis is to achieve different stable juggling patterns, whereas all different pattern permutations should be possible to reach. Therefore, it is essential to know which stable patterns are feasible at all, before an algorithm to actually attain the desired patterns can be derived. Similar to [7] we introduce

Definition 1. *An orbit of the impact map* (2.13) *is called an l-periodic orbit of order k, a* $\mathcal{P}_l^k$*-orbit, if it holds that*

$$\begin{pmatrix} t_{n+l} \\ \dot{x}^-_{B,n+l} \end{pmatrix} = \begin{pmatrix} t_n \\ \dot{x}^-_{B,n} \end{pmatrix} + \begin{pmatrix} k\xi \\ 0 \end{pmatrix}, \quad l,k \in \mathbb{N}, \quad \forall n \in \mathbb{Z}, \quad t_0 = 0, \tag{2.18}$$

where ξ *is the paddle period and the notation explained in Fig. 2.2 is used.*

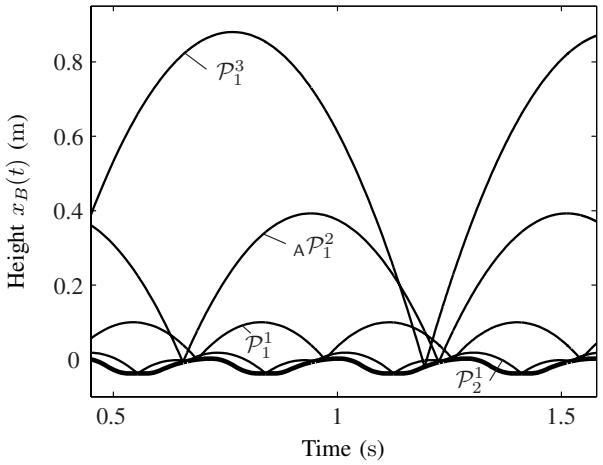

Figure 2.5: Examples of periodic orbits

To identify the feasible $\mathcal{P}_l^k$-orbits using the BJR, i.e. using the given paddle trajecotry in Section 2.2.1, a numerical approach is considered. A ball with a randomly chosen height in the range of 0 and 2 meters, which represents all physically feasible inital conditions of the ball denoted $\mathbf{x_B}(0)$, is dropped and simulated forward. After a large number of impacts, the ball has either reached a certain periodic orbit or it is classified as unstable. We have to indicate that the assumption is made that a ball cannot jump off the paddle anymore. Once it lies on the paddle, i.e. as soon as a ball rests on the paddle's surface, it is classified as unstable.
Because the BJR is physically limited to a juggling height of 2 meters, a relation between apex heights of $\mathcal{P}_1^k$-orbits is useful. The $\mathcal{P}_1^1$-orbit has the same period as the paddle. Let h_1 be the apex height for the $\mathcal{P}_1^1$-orbit, then the apex height h_k for a $\mathcal{P}_1^k$-orbit is, according to (2.18),

$$h_k = \frac{1}{2} g \underbrace{\xi_k^2}_{(k\xi)^2} = k^2 h_1, \tag{2.19}$$

where ξ_k is the period of the $\mathcal{P}_1^k$-orbit. The stabilizing paddle trajectory in Section 2.2.1 is characterized by the apex height h_1 of the $\mathcal{P}_1^1$-orbit. Having the relation (2.19) and an upper bound for the juggling height of 2 meters, a range for h_1 can

be determined where the feasible orbits are analyzed. We assume that at least the achievement of the $\mathcal{P}_1^3$-orbit should be possible. Therefore, it is necessary that

$$h_1 \leq \frac{2}{k^2} = \frac{2}{9} = 0.2222. \tag{2.20}$$

Executing the simulation specified above leads to Fig. 2.6, where the x-axis is proportional to the paddle frequency that is needed to reach the descripted height h_1. The five branches of Fig. 2.6 represent the different periodic orbits that can be reached, by the chosen paddle frequencies. The two lowest branches belong to the $\mathcal{P}_2^1$-orbit which has two different apex heights within one paddle period, as can be seen in Fig. 2.7(d). The remaining three branches describe the $\mathcal{P}_1^1$-,$\mathcal{P}_1^2$- and $\mathcal{P}_1^3$-orbit.

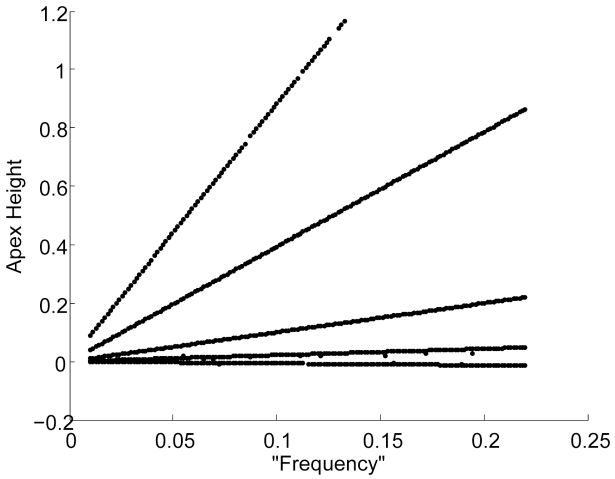

Figure 2.6: Feasible period orbits for varying frequency

We choose a frequency with an apex height $h_1 = 0.1$ meter and accordingly a maximum height $h_3 = 0.9$ meter.
Having four different periodic orbits that are feasible by the BJR, there is another possible distinction of juggling pattern within one orbit. For the $\mathcal{P}_1^2$- and $\mathcal{P}_1^3$-orbit there are phase shifts possible, as shown in Fig. 2.7(b). For the $\mathcal{P}_1^2$-orbit we denote them by ${}_{\mathsf{A}}\mathcal{P}_1^2$ and ${}_{\mathsf{B}}\mathcal{P}_1^2$. For the $\mathcal{P}_1^3$-orbit it will be shown in Section 3.3.2 why we neglect the phase shifting for that specific periodic orbit.

Figure 2.7 shows all feasible periodic orbits by the BJR, whereas in the following chapter an algorithm will be derived to reach any choice out of these orbits for any number of balls between one and four.

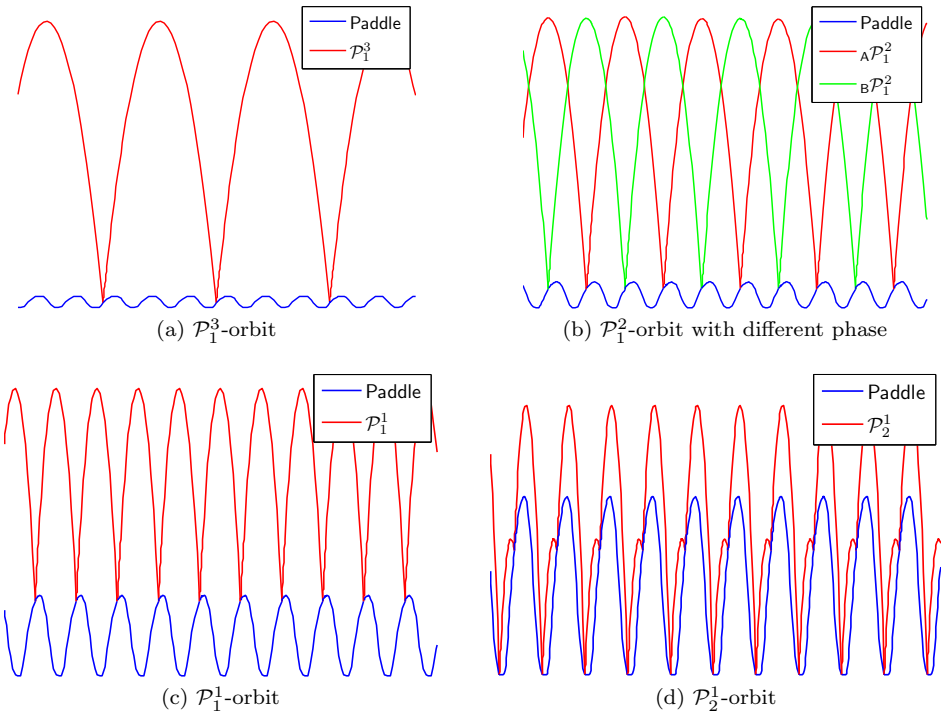

(a) $\mathcal{P}_1^3$-orbit (b) $\mathcal{P}_1^2$-orbit with different phase

(c) $\mathcal{P}_1^1$-orbit (d) $\mathcal{P}_2^1$-orbit

Figure 2.7: Feasible periodic orbits of the BJR

Chapter 3

First Algorithm - Map for Basin of Attraction

In this chapter, an algorithm is derived which achieves the given task in Section 1.3. Its main concept is a 'stability map' which is precomputed and can be used to estimate initial condidtions created by the chaos paddle movement leading to a specific periodic orbit. Several interpolation algorithms will be presented to estimate stability of an initial condition in the discrete 'stability map'. Last but not least, simulation results are presented and discussed.

First of all, the strategy is explained for one ball, i.e. there is one ball that has to achieve a desired periodic orbit. In Section 3.4, the control strategy is extended to the case of juggling multiple balls with different rhythmic patterns. Briefly explained, the control algorithm is looking for a time t_s where the paddle trajectory can be switched from the chaos to the stable mode, resulting in the desired periodic orbit as it is graphically explained in Fig. 3.1.

3.1 Basin of Attraction

At first, some definitions are needed which are similar to [10]:

Definition 2. $\mathbf{x}^*$ *is an attracting fixed point, if all trajectories that start near* $\mathbf{x}^*$ *approach it as* $t \to \infty$*. That is* $\mathbf{x}(\mathbf{t}) \to \mathbf{x}^*$ *as* $t \to \infty$*.*

Definition 3. *Given an attracting fixed point* $\mathbf{x}^*$*, its basin of attraction is defined to be the set of initial conditions* $\mathbf{x_0}$ *such that* $\mathbf{x}(\mathbf{t}) \to \mathbf{x}^*$ *as* $t \to \infty$*.*

The main idea of the control algorithm is to separate the problem into two parts, as shown in Fig. 3.1. There is a first part, where the ball is excited such that it enters a desired basin of attraction. In other words, the first part has the goal to generate adequate initial conditions for the ball. If we consider multiple balls, we additionally need to break the symmetry of the balls, i.e. we need to separate them. This part will be extensively treated in Section 3.3.
In the second part, the paddle movement follows the stabilizing trajecotry of Section 2.2.1. Using this paddle trajectory, the stability analysis is performed. In this part, we actually reach the desired periodic orbits. Our genearal idea is that we want to know the set of all physically feasible initial conditions of the ball that lead to a specific periodic orbit. Having this set we can easily decide for which ball states at a potential switching time t_s we can switch the paddle's trajectory to the second mode such that the desired periodic orbit results. In other words, what needs to be

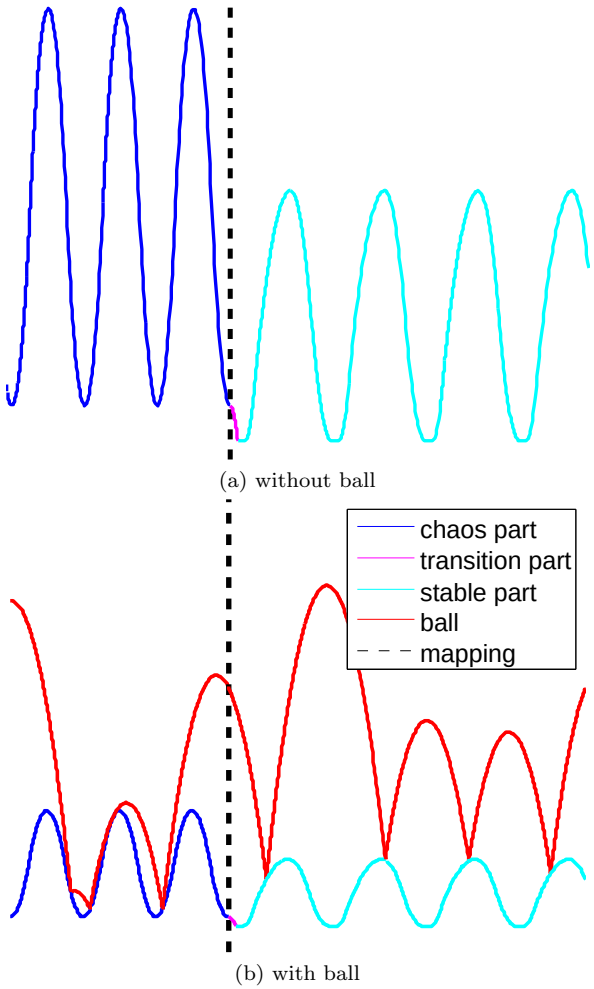

(a) without ball

(b) with ball

Figure 3.1: The blue trajectory correspondes to the chaos trajectory. To switch to the stabilizing paddle trajectory (cyan) we need a small transition part (pink).

known, are the basins of attraction for each periodic orbit.

At first, the set of all physically possible initial ball conditions for the BJR has to be determined. Using the limitation of the apex height of $h_{min} = -A$, $h_{max} = 2$ meters and (2.4), the maximum ball height is determined by standard methods:

$$\frac{d}{dt}x_B(t) = -gt + \dot{x}_B(0) \stackrel{!}{=} 0 \quad \Rightarrow t = \frac{\dot{x}_B(0)}{g} \tag{3.1}$$

$$\frac{d^2}{dt^2}x_B(t) = -g < 0 \quad \Rightarrow \text{Maximum} \tag{3.2}$$

Using (2.4) and (3.1) an inequality is derived as

$$x_{B,max} = \frac{1}{2}\frac{\dot{x}_B^2(0)}{g} + x_B(0) \stackrel{!}{<} h_{max}. \tag{3.3}$$

Now a relation between the inital conditions $x_B(0)$ and $\dot{x}_B(0)$ using (3.3) becomes

$$|\dot{x}_B(0)| < \sqrt{2g(h_{max} - x_B(0))}, \tag{3.4}$$

which is a region with a parabolic curve as boundary that describes the set of all physically feasible initial conditions

$$R = \{\mathbf{x_B}(0) \in \mathbb{R}^2 : |\dot{x}_B(0)| < \sqrt{2g(h_{max} - x_B(0))}, \quad h_{min} \leq x_B(0) \leq h_{max}\}, \tag{3.5}$$

which is shown in Fig. 3.2.

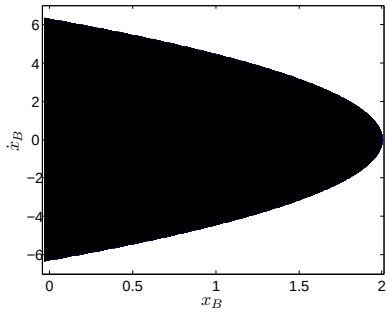

Figure 3.2: Set R of all physically feasible initial conditions at switching time t_s

The basin of attraction is numerically computed by applying a fine grid to the set R and simulating each grid point. A grid point, i.e. an initial condition, which leads to a certain periodic orbit, is indicated by a red grid point, whereas a grid point, i.e. an initial condition, which does not converge to a desired periodic orbit is marked by a green grid point. The computation is caried out in the following way: A certain initial condition is taken and then the ball's trajectory under the stabilizing paddle trajectory is computed. This is done for 100 impacts. If two impacts occur within a tolerance ϵ, i.e. $t_{i+1} - t_i < \epsilon$, where t_i denotes the time when the i^{th} impact occurs, the simulation is stopped and the considered pair of initial conditions marked with a green point. As mentioned the assumption is made that a ball cannot jump off the paddle anymore, once it is at rest. If no ball is at rest after 100 impacts and if the desired periodic obit is reached, the initial condition is marked with a red point. The detection of which periodic orbit is reached is easy, since each periodic orbit is fully characterized by its period, apex height and phase, as can be seen in Fig. 2.7. Finally, the set of all red points is equal to the (discrete) basin of attraction for a certain periodic orbit, which is plotted in Fig. 3.3.
Although this is rather computationally intensive, it should also be noted that once the basin of attraction is known, it allows a control strategy that is computationally cheap and can be executed in realtime what is exactly needed for an implementation with the BJR.

Taking a closer look at the basins of attraction in Fig. 3.3, it can be noticed that for the ${}_{\mathsf{A}}\mathcal{P}_1^2$-, ${}_{\mathsf{B}}\mathcal{P}_1^2$-, and $\mathcal{P}_1^1$-orbit, there is in each case one large connected region. It should be clear by considering the location of each region and can easily be verified by simulation that these large connected regions contain the nominal initial condition. The nominal initial condition is characterized by the fact that the first impact velocity and impact position exactly match the steady state values of the particular periodic orbit. The nominal initial condition is marked with a black star in Fig. 3.3.
In Fig. 3.3(a), there are three connected regions with roughly the same size, due to the fact that for the $\mathcal{P}_1^3$-orbit, three phase shifts are possible. One could think of distinguishing between a ${}_{\mathsf{A}}\mathcal{P}_1^3$-, ${}_{\mathsf{B}}\mathcal{P}_1^3$- and ${}_{\mathsf{C}}\mathcal{P}_1^3$-orbit. It will be explained in Section 3.3.2 why we avoid this distinction and unite the ${}_{\mathsf{A}}\mathcal{P}_1^3$-, ${}_{\mathsf{B}}\mathcal{P}_1^3$- and ${}_{\mathsf{C}}\mathcal{P}_1^3$-orbit to the $\mathcal{P}_1^3$-orbit.

The basin of attraction for the $\mathcal{P}_2^1$ orbit, which is illustrated in Fig. 3.3(e) contains no major connected region. This already suggests, what will be explained in more detail in Section 3.2.5, that it is the most challenging juggling pattern to reach and that it is highly sensitive.

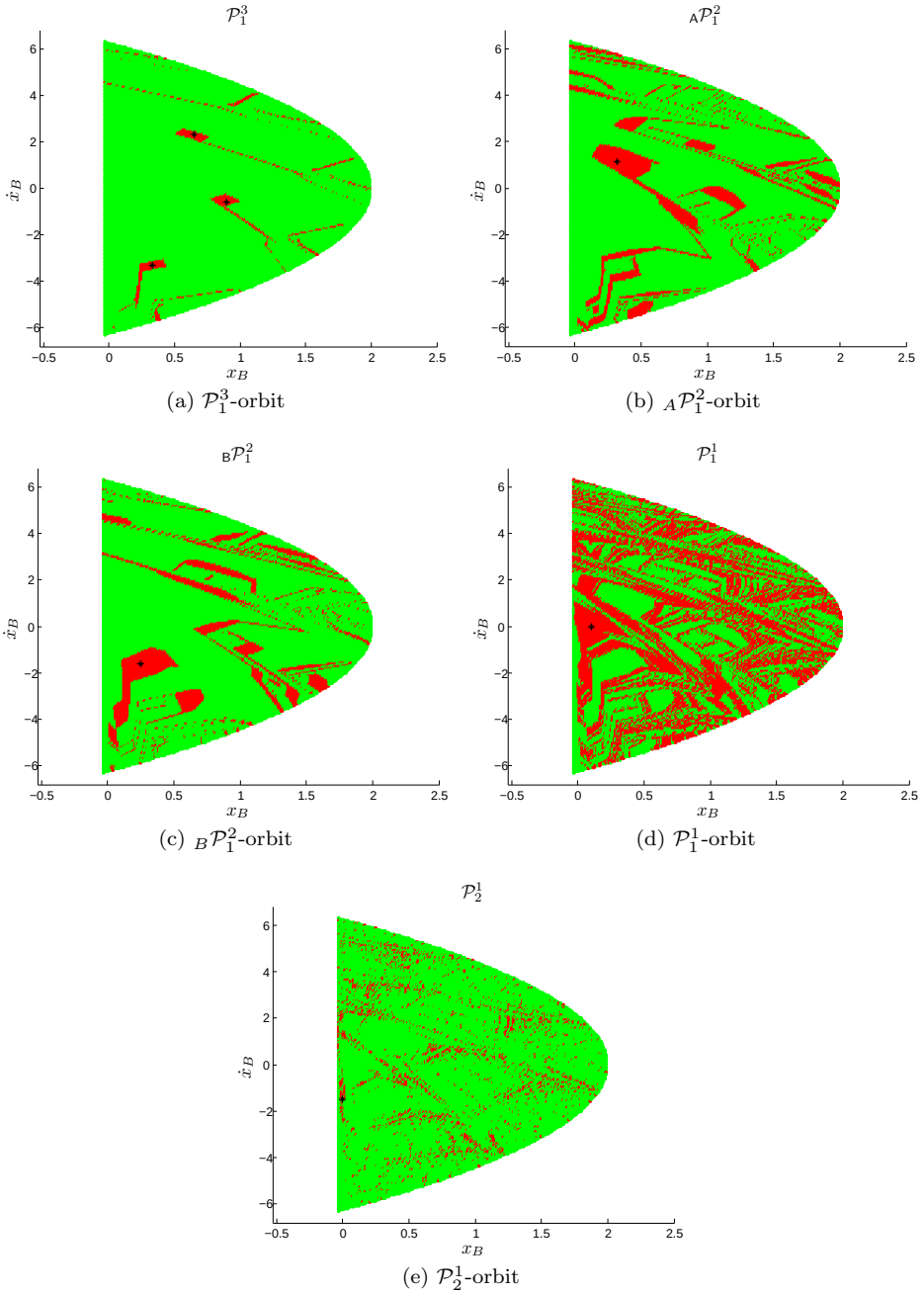

(a) $\mathcal{P}_1^3$-orbit

(b) $_A\mathcal{P}_1^2$-orbit

(c) $_B\mathcal{P}_1^2$-orbit

(d) $\mathcal{P}_1^1$-orbit

(e) $\mathcal{P}_2^1$-orbit

Figure 3.3: Basin of attraction

3.2 Interpolation

Since the basin of attraction was computed by simulating different initial conditions represented by grid points, a measured initial condition, that has to be classified by

the computed basin of attraction will never exactly match one of the grid points. Therefore, to classify a measured initial condition we use an interpolation algorithm. To the best of our knowledge, there are no previous results in the literature that solve this specific interpolation problem. However, we introduce four different interpolation algorithm and discuss them relating to performance. The following four interpolation algorithms are presented:

- Nearest Neighbour Algorithm (NNA)
- Weighted Average Algorithm (WAA)
- Connectivity Algorithm (CA)
- Robust Algorithm (RA)

Being able to describe the derived algorithms some definitions from graph theory are needed. They are analog to [11]:

Definition 4. *A graph is a pair* $G = (V, E)$ *of sets such that* $E \subseteq \binom{V}{2} := \{\{x, y\} | x, y \in V, x \neq y\}$. *The elements of* V *are the vertices (or nodes) of the graph* G*, the elements of* E *are its edges.*

Definition 5. *For a vertex* $v \in V$ *of a graph* G*, let* $\Gamma(v) := \{u \in V | \{u, v\} \in E\}$ *be its neighbourhood*

Definition 6. *Let* $\biguplus_{i=1}^{k} V_i$ *be a partition of* V*, such that two vertices* u *and* v *are connected by a path iff they lie in the same partition. The subgraphs* $G[V_i]$ *are called connected components of* G*.*

3.2.1 Nearest Neighbour Algorithm

As a basic idea, the basin of attraction is understood as a mesh graph $M_{m,n}$, where the vertices are the simulated grid points. Let u be a given inital condition that needs to be classified. Therefore, u is mapped to the set of feasible initial conditions R and the relevant section of $M_{m,n}$ i.e. the neighbourhood is going to be considered for the classification, as it is shown in Fig. 3.4(a).

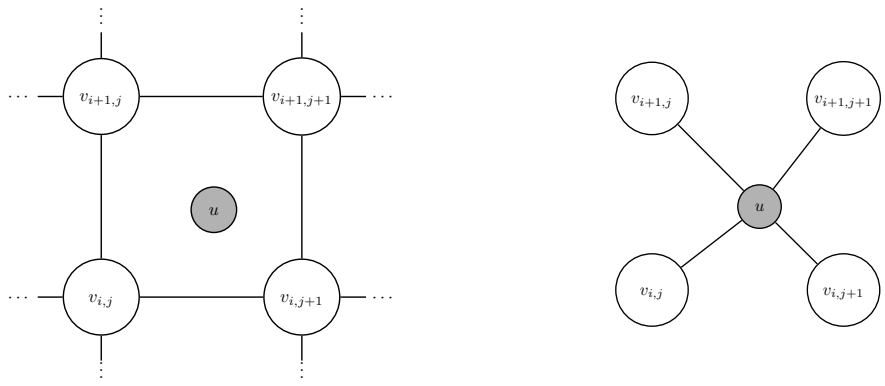

(a) Mesh graph $M_{2,2}$ (b) Star graph S_4

Figure 3.4: Grid points v with measured data point u

A justification for the handling of the problem as a graph could be sketched as follows: There exists a bijective mapping

$$\begin{aligned} \varphi: \quad & V_{M_{m,n}} \to R, \\ & v_{i,j} \mapsto \{x_{B,j}, \dot{x}_{B,i}\} \end{aligned} \tag{3.6}$$

by construction of the discrete set R that maps each vertex $v_{i,j}$ of $M_{m,n}$ to a grid point in R. Let $k, l \in \mathbb{R}_+$, but $\notin \mathbb{N}$ and let $\{x_{B,l}, \dot{x}_{B,k}\}$ be the measured initial conditions. If we now choose $i < k < i+1$ and $j < l < j+1$ the closest four inital condition pairs are uniquely determined. Hence, by applying the bijection φ^{-1} the four vertices are unique as well:

$$\begin{pmatrix} \{x_{B,j}, \dot{x}_{B,i+1}\} & \{x_{B,j+1}, \dot{x}_{B,i+1}\} \\ \{x_{B,j}, \dot{x}_{B,i}\} & \{x_{B,j+1}, \dot{x}_{B,i}\} \end{pmatrix} \xrightarrow{\varphi^{-1}} \begin{pmatrix} v_{i+1,j} & v_{i+1,j+1} \\ v_{i,j} & v_{i,j+1} \end{pmatrix} \tag{3.7}$$

This analysis allows to consider the description of the problem as a graph, as showed in Fig. 3.4, where each vertex can be uniquely mapped to a pair of initial conditions of R.

To describe the NNA, the star graph S_4 as depicted in Fig. 3.4(b) is considered. If we look at the set of initial conditions $\{x_{B,j}, \dot{x}_{B,i}\}$ as a vector $\begin{pmatrix} x_{B,j} \\ \dot{x}_{B,i} \end{pmatrix}$ each edge $e \in E$ of S_4 can be assigned with a weight $W(e) \in \mathbb{R}$, that is defined as

$$W(e) := \{\frac{1}{\|\varphi(u) - \varphi(v)\|} | \{u, v\} = e \in E\}, \tag{3.8}$$

where the denominator is unequal zero, because $k, l \notin \mathbb{N}$.

Now, a formulation of the NNA can be given as

$$\mathscr{S}(u) := \mathscr{S}(\arg\min_{v \in \Gamma(u)} W(\{u, v\})), \tag{3.9}$$

where

$$\mathscr{S}(v) = \begin{cases} 1, & \text{if } \varphi(v) \text{ is part of the basin of attraction} \\ 0, & \text{otherwise} \end{cases} \tag{3.10}$$

is the indicator function.

Although the theoretical derivation of the NNA looks rather complex, it is a trivial exercise to implement it using MATLAB. The theoretical description is needed on the one hand to be formally correct and on the other hand, it will be used later to describe more sophisticated interpolation algorithms.

3.2.2 Weighted Average Algorithm

The WAA is roughly speaking an extension of the NNA. It will improve some of the drawbacks that the NNA has. One major drawback, that will be improved, is that the NNA is a greedy algorithm, because it only looks for the locally closest neighbour. Hence, all the available information about the 'stability' of the other neighbours is not considered, which should intuitively lead to a limited performance. As an example which highlights this problem one could imagine a measured point lying just outside a stable region has to be classified. Because its nearest neighbour

is the boundary point of a stable section it is classified as 'stable'. However, it will be 'unstable'. This problem might be avoided by considering the whole neighbourhood of the measured point. If we define $\Gamma_S(u) := \{v \in V | \{u, v\} \in E \wedge \mathscr{S}(v) = 1\}$ as the stable neighbourhood of u, the weighted average of a measured point u

$$\mathscr{A}(u) := \frac{\sum\limits_{v \in \Gamma_S(u)} W(\{u, v\})}{\sum\limits_{v \in \Gamma(u)} W(\{u, v\})} \tag{3.11}$$

can be defined, where W is the weight from (3.8).
Summing up, a measured point u can be classified by the WAA in the following two steps:

1. compute the weighted average $\mathscr{A}(u)$
2. $\mathscr{S}(u) := \begin{cases} 1, & \text{if } \mathscr{A}(u) > \alpha \\ 0, & \text{otherwise} \end{cases}$

The parameter $\alpha \in [0, 1]$ indicates how demanding the classification is to the neighbourhood to of a point u to classify it as 'stable'. For example if α is set to 1 the whole neighbourhood, i.e. all four points, have to be 'stable' such that u is classified as 'stable', whereas for $\alpha = 0$ u with any neighbourhood is classified as 'stable', which is of course useless. Figure 3.5 shows some arbitrarily chosen examples for the WAA, where the light red area represents the domain where all measured points will be classified as being part of the basin of attraction. Based on experience, we choose the design parameter α between 0.8 and 0.9 to get reasonably reliable results.

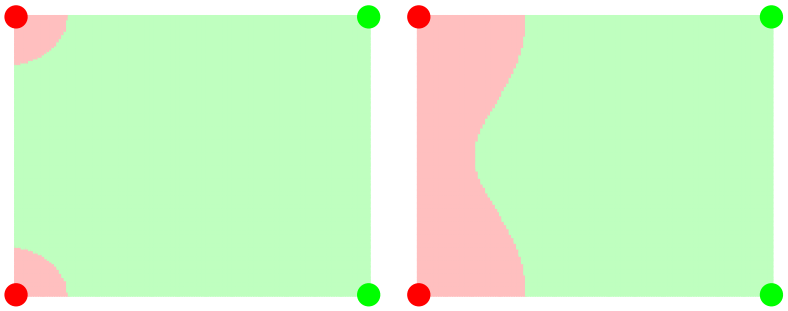

(a) $\alpha = 0.8$ (b) $\alpha = 0.65$

(c) $\alpha = 0.35$ (d) $\alpha = 0.5$

Figure 3.5: Examples for WAA

3.2.3 Connectivity Algorithm

This algorithm is based on the assumption that in the basins of attraction in Fig. 3.3, stable regions are often connected. Therefore, the main idea of the CA is to put

more emphasis on connectivity. To explain how the classification is made by the CA, it is convenient to look at two examples. In Fig. 3.6 the light red area represents the domain where all measured points will be classified as being part of the basin of attraction.

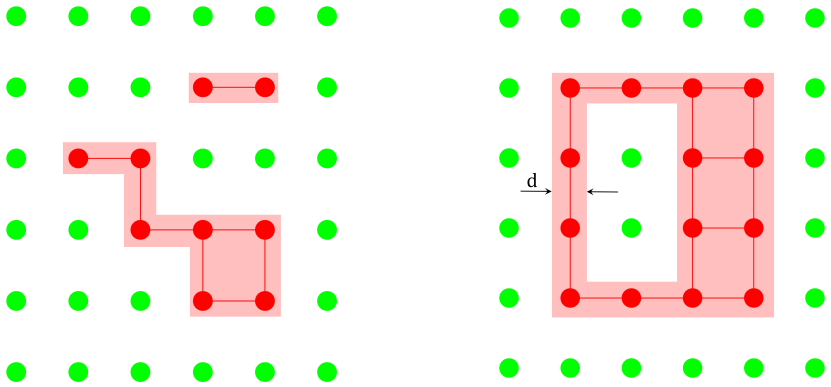

(a) Two connected components $G[V_i]$ and $G[V_j]$

(b) One connected component $G[V_i]$

Figure 3.6: Examples for CA

The mathematical description of the CA is based on the two former algorithms, that are presented in Section 3.2.1 and 3.2.2. However, to keep it as simple as possible, a slight different notation in the mesh graph $M_{2,2}$ is used, as can be seen in Fig. 3.7. Now, an explicit formulation of the CA is given, i.e. a method of how to classify a

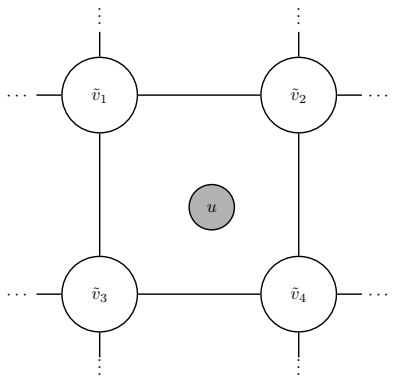

Figure 3.7: Mesh graph $M_{2,2}$ with notation for CA

measured vertex u:

(i) if $\tilde{v}_i \in G[V_k]$, for $i = 1, 2, 3, 4$ and fixed k
$\Rightarrow \mathscr{S}(u) = 1$

(ii) if $\{\tilde{v}_i, \tilde{v}_j\} \in E_{M_{2,2}} \wedge \{\tilde{v}_i, \tilde{v}_j\} \in G[V_k]$, for $i, j \in \{1, 2, 3, 4\}, i \neq j$ and fixed k
$$\Rightarrow \mathscr{S}(u) = \begin{cases} 1, & \text{if } \min|\varphi(u) - \varphi(\tilde{v}_i)| < d \\ 0, & \text{otherwise} \end{cases}$$

(iii) if $\tilde{v}_i \in G[V_k]$, for $i \in \{1, 2, 3, 4\}$ and variable k
$$\Rightarrow \mathscr{S}(u) = \begin{cases} 1, & \text{if } \max|\varphi(u) - \varphi(\tilde{v}_i)| < d \\ 0, & \text{otherwise} \end{cases}$$

Basically the CA distinguishes three cases considering the mesh graph in Fig. 3.7: In case (i), all four neighbours $\tilde{v}$ of a measured point u belong to the basin of attraction. In case (ii), two adjacent grid points are parts of the basin of attraction, similar to the upper connected component in Fig. 3.6(a). Therefore, a bar with thickness d around the two adjacent points has to be considered. Finally in case (iii), only one vertex of the four neighbours is part of the basin of attraction. As shown in Fig. 3.6, d is the range around a single 'stable' point that is classified as belonging to the basin of attraction and is a constant design parameter.

3.2.4 Robust Algorithm

The main goal of the RA is to be robust, i.e. even for small variations of the measured inital condition to the real initial condition, if the paddle trajectory is switched from chaos into the stabilizing mode it should result the desired periodic orbit. Furthermore, the errors due to the unknown edges of the basins of attraction should be reduced. This is done by considering an extended neighbourhood of a measured point u. As the algorithm is not very complicated, it can be explained in words:

A given measured point u is classified as being part of a particular basin of attraction if and only if all vertices that belong to its extended neighbourhood, as defined in Fig. 3.8, are grid points of this basin of attraction.

As the initial conditions classified by this algorithm will clearly be more robust, the drawback of this method is that many possible switching points are missed because only a partial neighbourhood was in the basin of attraction. Especially if multiple balls have to reach a challenging juggling pattern this leads to rather long switching times t_s. Furthermore, as can be seen in Fig. 3.3(e), for the $\mathcal{P}_2^1$ orbit there might not exist such a big neighbourhood in the domain of attraction, so we might lose one periodic orbit using the RA.

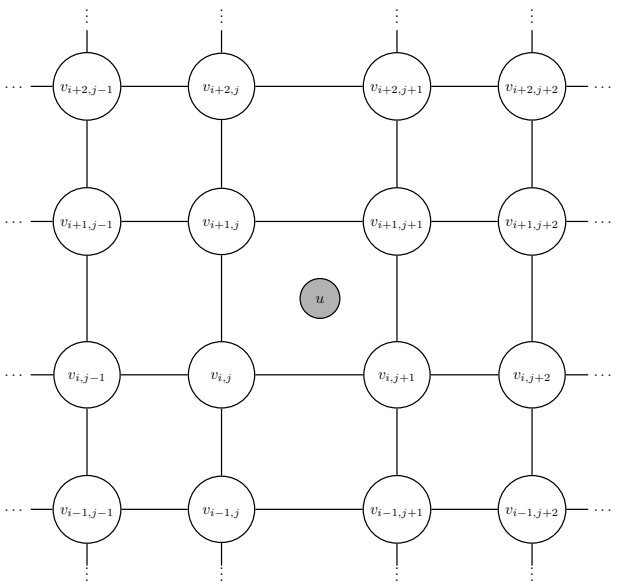

Figure 3.8: Mesh graph $M_{4,4}$

3.2.5 Performance Evaluation

In order to compare the performance of the derived algorithms, a numerical experiment is conducted. 100 different initial conditions are randomly chosen. Each algorithm is set the task to reach one specific periodic orbit for each of the 100 initial conditions. As can be seen in Tab. 3.1, the column 'reliability' indicates how many of the 100 initial conditions resulted in the desired periodic orbit, by each particular interpolation algorithm, divided by 100. Whereas $\bar{t}_s$ denotes the average switching time in seconds.

Table 3.1: Performance evaluation

	NNA		WAA		CA		RA	
	reliability	$\bar{t}_s$	reliability	$\bar{t}_s$	reliability	$\bar{t}_s$	reliability	$\bar{t}_s$
$\mathcal{P}_1^3$	0.58	18.1	0.83	30.2	0.8	22.3	0.98	43.3
${}_{\mathsf{A}}\mathcal{P}_1^2$	0.88	1.7	0.99	2.0	0.99	2.0	1	2.4
${}_{\mathsf{B}}\mathcal{P}_1^2$	0.82	1.8	0.95	2.2	0.97	2.4	1	2.7
$\mathcal{P}_1^1$	0.81	1.0	0.91	1.1	0.89	1.0	0.98	1.7
$\mathcal{P}_2^1$	0.45	2.7	0.79	13.3	0.76	15.4	/	/

It can be seen that a set of inital conditions that is classified by the NNA often leads to the wrong periodic orbit. Although the NNA requires the shortest switching times, its reliability is such low that it has to be stated as an useless interpolation algorithm for the desired purpose.

The WAA and the CA have similar performace. Both average switching time and reliabilty only differ few from each other. Therefore, it cannot clearly be estimated which interpolation algorihm should be preferred. However, it is intriguing that for almost each periodic orbit one of those two interpolation algorithm has slightly better reliability. Hence, one could try to combine the two algorithms such that for each periodic orbit the specific better algorithm will be used.

The RA satisfies most. Even if the waiting times for the switching from the chaos paddle movement to the stabilizing trajectory are somewhat higher, compared to the ohter algorithms, its reliability is clearly the best. Therefore, the RA is - in spite of the fact to require larger waiting times - the prefered algorithm. Unfortunately, the basin of attraction of the $\mathcal{P}_2^1$ orbit cannot be interpolated using the RA, because - as supposed in Section 3.2.4 - there is no connected region in the basin of attraction, which is big enough. Hence, the interpolation for the $\mathcal{P}_2^1$ orbit is executed with the WAA, because of a small advantage in reliability and switching time in contrast to the CA, as shown in Fig. 3.9(e).

Concluding, we can state that a tradeoff between switching time and reliability is required, where the reliability, however, is of higher interest. In Chapter 4, a completely new approach is presented, with the main goal to reach a higher robustness, i.e. reliability.

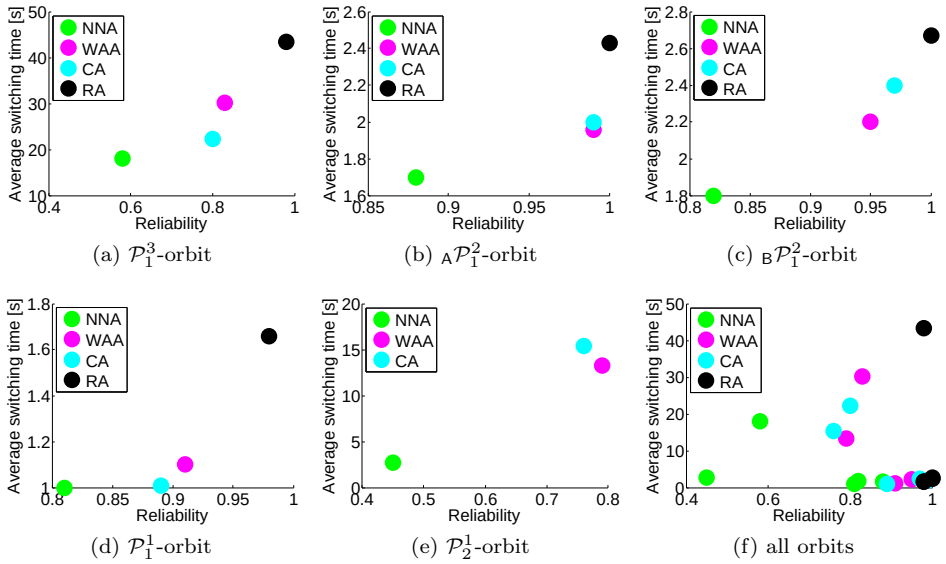

(a) $\mathcal{P}_1^3$-orbit (b) ${}_A\mathcal{P}_1^2$-orbit (c) ${}_B\mathcal{P}_1^2$-orbit

(d) $\mathcal{P}_1^1$-orbit (e) $\mathcal{P}_2^1$-orbit (f) all orbits

Figure 3.9: Overview performance

3.3 Introducing Chaos

As the second part of the split-up problem, the stabilizing paddle trajecotry is analyzed. This section gives an insight into the frist part - the chaos excitation. It was already mentioned that the main goal of the chaos trajectory is to reach a desired domain in the basin of attraction. Another requirement of the chaos excitation is to 'break symmetries', i.e. if a stable juggling pattern is reached, with two or more balls in the same periodic orbit, the balls follow the same trajectory and have only very little differences in the states. If we now want to realize another juggling pattern, we want to switch the paddle trajectory into the chaos mode and execute the described algortihm to perform the desired new pattern. Therefore, a paddle trajectory is needed such that the balls get separated form each other. Otherwise the balls would follow almost identical trajectories and it would not be possible to realize different periodic orbits for different balls. As the balls always have uncertainties due to parameter noise, a system behavior that exhibits sensitive dependence on initial conditions would be perfectly suited to separate the balls. These two requirements lead to the idea of choosing a paddle trajectory that produces chaotic motion of the balls and that we call chaos paddle trajectory.

As a reminder to the reader and because there are different definitions of what chaos is, we define analog to [10]:

Definition 7. *Chaos is aperiodic long-term behaviour in a deterministic system, that exhibits sensitive dependence on initial conditions.*

'Aperiodic long-term behaviour' means that there are trajectories which do not settle down to fixed points or periodic orbits as $t \to \infty$. To be able to describe exactly the basic ideas, that are used in this section another term is needed, which is taken from [10]:

Definition 8. *An attractor is defined as a closed set $\mathcal{A}$ with the following properties:*

1. *$\mathcal{A}$ is an invariant set: any trajectory $x(t)$ that starts in $\mathcal{A}$ stays in $\mathcal{A}$ for all time*

2. *$\mathcal{A}$ attracts an open set of initial conditions: there is an open set $\mathcal{U}$ containing $\mathcal{A}$ such that if $x(0) \in \mathcal{U}$, then the distance from $x(t)$ to $\mathcal{A}$ tends to zero as $t \to \infty$. This means that $\mathcal{A}$ attracts all trajectories that start sufficiently close to it.*

3. *$\mathcal{A}$ is minimal: there is no proper subset of $\mathcal{A}$ that satisfies conditions 1 and 2.*

Definition 9. *A strange attractor is defined to be an attractor that exhibits sensitive dependence on initial conditions.*

Now, we justify why the paddle trajectory from Section 2.2.2 produces chaotic behaviour of the bouncing ball system. In Fig. 3.10 two different trajectories are shown that differ in position by 0.00001 meters at the zeroth impact. After just six impacts the two trajecotries show no resemblance anymore. This is a descriptive justification for the sensitive dependence on initial conditions of the given system. The aperiodic long-term behaviour of the system can be seen in Fig. 3.12, where the states at potential switching points are plotted for 100,000 impacts. Finally, the system is deterministic since it has no random or noisy inputs or parameters. According to Def. 7, the system with the chosen paddle trajectory is chaotic.

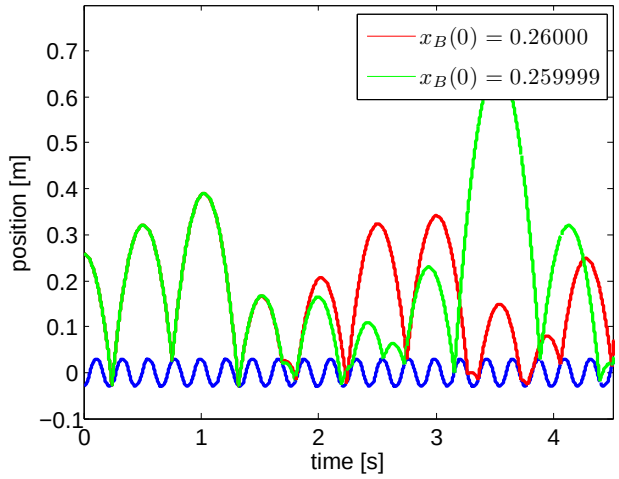

Figure 3.10: Sensitive dependence on initial conditions

3.3.1 Upper Bound for Height

As the BJR is limited to a maximum juggling height of h_{max}= 2 meters, the chaos paddle trajectory from Section 2.2.2 has to be chosen such that this limit will never be exceeded. In this section, an upper bound for the maximum juggling height is derived, which allows to choose an appropriate maximum stroke A for the chaos paddle trajectory.

Proposition 1. *For reasonable initial conditions and a paddle trajectory as given in Section 2.2.2 the following upper bound for the ball height holds:*
$x_B(t) \leq \frac{1}{g}(\frac{1+e_z}{1-e_z})^2 a_c A, \quad \forall t \in \mathbb{R}_+$

Proof. Let $\dot{\mathbf{x}}^+_{\mathbf{B},\mathbf{n}} := \begin{pmatrix} \dot{x}_B^+[0] \\ \dot{x}_B^+[1] \\ \vdots \\ \dot{x}_B^+[n] \end{pmatrix} \in \mathbb{R}^n, \dot{\mathbf{x}}^-_{\mathbf{B},\mathbf{n}} := \begin{pmatrix} \dot{x}_B^-[0] \\ \dot{x}_B^-[1] \\ \vdots \\ \dot{x}_B^-[n] \end{pmatrix} \in \mathbb{R}^n$ and $\dot{\mathbf{x}}_{\mathbf{P},\mathbf{n}} :=$

$\begin{pmatrix} \dot{x}_P[0] \\ \dot{x}_P[1] \\ \vdots \\ \dot{x}_P[n] \end{pmatrix} \in \mathbb{R}^n$, where $n \in \mathbb{N}_0$ indicates the impact number. According to [12], we use that in a normed vector space V, the triangle inequality

$$\|\mathbf{x}+\mathbf{y}\| \leq \|\mathbf{x}\| + \|\mathbf{y}\| \quad \forall \mathbf{x}, \mathbf{y} \in V \tag{3.12}$$

holds, where here the infinity norm $\|\mathbf{x}\|_\infty := \max_i |x_i|$ is used. Hence, using (2.8) and (3.12) leads to

$$\|\dot{\mathbf{x}}^+_{\mathbf{B,n}}\|_\infty = \|-e_z\dot{\mathbf{x}}^-_{\mathbf{B,n}} + (1+e_z)\dot{\mathbf{x}}_{\mathbf{P,n}}\|_\infty \leq e_z\|\dot{\mathbf{x}}^-_{\mathbf{B,n}}\|_\infty + (1+e_z)\underbrace{\|\dot{\mathbf{x}}_{\mathbf{P,n}}\|_\infty}_{\leq\sqrt{2a_cA}}. \tag{3.13}$$

The relation $\|\dot{\mathbf{x}}_{\mathbf{P}}\|_\infty \leq \sqrt{2a_cA}$ used in the last step can easily be verified considering (2.14). The assumption is made that the paddle's displacement is always small compared to the ball's maximum height. Therefore the update condition

$$\dot{x}^+_B[n] = \dot{x}^-_B[n+1], \quad n \in \mathbb{N}_0 \tag{3.14}$$

results. Using (3.13) and (3.14), the following scalar inequality can be derived:

$$\dot{x}^+_B[n] \leq \|\dot{\mathbf{x}}^+_{\mathbf{B,n}}\|_\infty \leq e_z\|\dot{\mathbf{x}}^+_{\mathbf{B,n-1}}\|_\infty + (1+e_z)\sqrt{2a_cA}. \tag{3.15}$$

We define

$$m[i] := \|\dot{\mathbf{x}}^+_{\mathbf{B,i}}\|_\infty, \quad i \in \mathbb{N}_0 \text{ and} \tag{3.16}$$

$$\alpha := (1+e_z)\sqrt{2a_cA}. \tag{3.17}$$

With (3.15) an iteration can be proceeded:

$$\begin{aligned} &m[1] \leq e_z m[0] + \alpha \\ &m[2] \leq e_z m[1] + \alpha \leq e_z^2 m[0] + \alpha e_z + \alpha \\ &m[3] \leq e_z m[2] + \alpha \leq e_z^3 m[0] + \alpha e_z^2 + \alpha e_z + \alpha \\ &\vdots \\ &m[n] \leq \alpha(\sum_{i=0}^{n-1} e_z^i) + e_z^n m[0]. \end{aligned} \tag{3.18}$$

Using the fact that the (non ideal) coefficient of restitution satisfies $0 < e_z < 1$, the geometric series (3.18) converges if the limit of n to infinity is taken, i.e.

$$m[n] \leq \frac{1-e_z^n}{1-e_z}\alpha + e_z^n m[0] \tag{3.19}$$

$$\lim_{n\to\infty} m[n] \leq \frac{1}{1-e_z}\alpha = \frac{1+e_z}{1-e_z}\sqrt{2aA} \tag{3.20}$$

This leads to the upper bound for the post impact velocity

$$\dot{\mathbf{x}}^+_{\mathbf{B,n}} \leq \frac{1+e_z}{1-e_z}\sqrt{2aA} \quad , \forall n \in \mathbb{N}_0. \tag{3.21}$$

Now, applying the equation for an uniform acceleration we get $x_B(t) \leq \frac{\|\dot{\mathbf{x}}^+_{\mathbf{B,n}}\|^2_\infty}{2g}$, $\forall t \in \mathbb{R}_+$ and therefore $x_B(t) \leq \frac{1}{g}(\frac{1+e_z}{1-e_z})^2 a_c A, \quad \forall t \in \mathbb{R}_+$. □

In particular, the upper bound for the maximum height does not depend on the initial conditions of the ball. It will be shown in the next section by simulation, that the upper bound is rather conservative. However, it is convenient to have the bound for an indication of how the maximum height changes when parameters are varied, i.e. one can see that the upper bound changes linearly with the maximum stroke A of the chaos paddle trajectory.

3.3.2 Strange Attractor - Parameter Evaluation

In this section, the design parameters for the chaos trajectory (2.14) - namely paddle acceleration a_c and maximum stroke A - are derived. The main idea is that the strange attractor of the system under the chaos trajectory should overlap as much as possible with the basin of attraction of the system excited with the stabilizing paddle trajectory. Therefore, the strange attractor of the system excited with the chaos trajectory is numerically determined and optimized for the described parameters. This is done by starting with a randomly chosen set of initial conditions and simulating the system for 10,000 impacts, where at each potential switching point, the ball's state is plotted.

At first, the paddle acceleration is derived. Therefore, the maximum stroke is fixed to a certain value and a_c is varied, where due to the physical limitation of the BJR, the paddle acceleration cannot be chosen greater than $2g$. As shown in Fig. 3.11, between $a_c = g$ and $a_c = 1.25g$ the chaotic behaviour of the systems starts. The strange attractor gets bigger as the paddle acceleration is increased. Therefore, it seems reasonable to choose the highest, physically possible acceleration, i.e. $a_c = 2g$.

Having fixed the paddle acceleration to $a_c = 2g$, a well-founded value for the maximum stroke A is derived. It can easily be shown by simulation that A has to be chosen within the range [0, 0.03], because of the limited maximum height of the ball. However, if the upper bound derived in Section 3.3.1 is used, the range [0, 0.0124] is obtained, which is - as already mentioned - too conservative and will not be used here. Roughly spoken, a value for the parameter A is sought such that the strange attractor of the system under the chaos trajectory overlaps as much as possible with the basin of attraction of the system excited by the stabilizing paddle trajectory. To determine numerically whether a point of the strange attractor matches with the basin of attraction in Fig. 3.3, the particular point is classified using an appropriate interpolation algorithm from Section 3.2. In Tab. 3.2, each point of the strange attractor for each periodic orbit was classified by the WAA. The value in the table is the number of points belonging to the strange attractor that overlap with the particular basin of attraction, divided by the number of all points in the strange attractor. In Tab. 3.3 the interpolation is performed with the CA.

It can be noticed looking at either of the tables that by increasing the paramter A, the overlapping of the strange attractor with the basin of attraction of the $\mathcal{P}_1^1$- and $\mathcal{P}_2^1$-orbit decreases, whereas the remaining three periodic orbits get a higher overlapping. As the $\mathcal{P}_1^1$-orbit is trivial to reach and as the $\mathcal{P}_2^1$-orbit will be highly challenging, up to nearly impossible, to reach, we prefer a high value for the parameter A. Therefore, A is chosen to be 0.03. In Fig. 3.12, the strange attractor for the chaos paddle trajecotry with the parameters determined in this section is plotted using 100,000 samples.

A visualization of the overlapping is given in Fig. 3.13, where the strange attractor

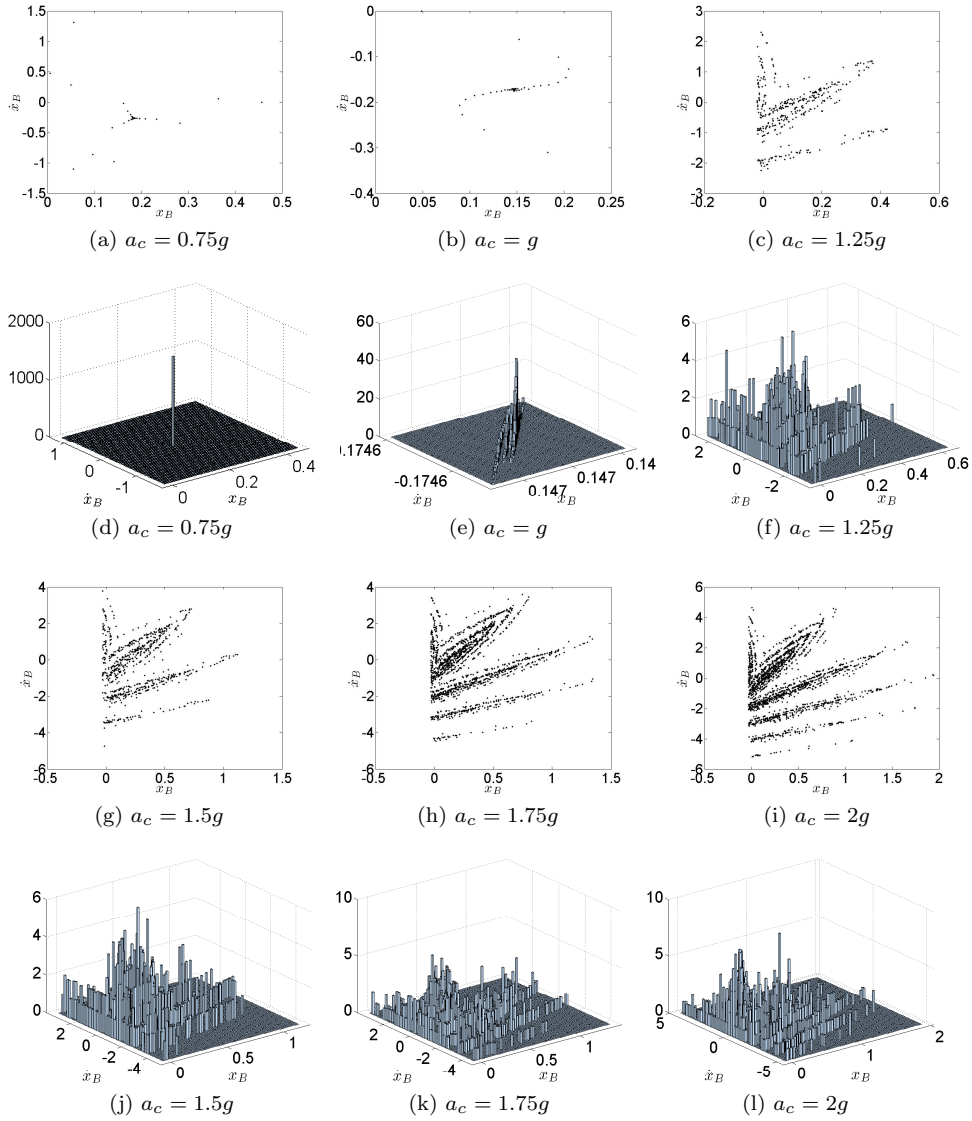

(a) $a_c = 0.75g$ (b) $a_c = g$ (c) $a_c = 1.25g$

(d) $a_c = 0.75g$ (e) $a_c = g$ (f) $a_c = 1.25g$

(g) $a_c = 1.5g$ (h) $a_c = 1.75g$ (i) $a_c = 2g$

(j) $a_c = 1.5g$ (k) $a_c = 1.75g$ (l) $a_c = 2g$

Figure 3.11: Strange attractors and their histograms

for the chosen parameters is plotted over the basins of attraction for each periodic orbit. Now, we can justify why we do not consider phase shifts in the $\mathcal{P}_1^3$-orbit. Two out of the three connected domains in the basin of attraction for the $\mathcal{P}_1^3$-orbit are hardly reachable with the chosen strange attractor, what can be seen in Fig. 3.13(a). Therefore, it makes no sense to distinguish between this three connected regions which belong to the three different phase shifts that are possible.

3.4 Algorithm and Extension to Multiple Balls

In this section, we bring the two parts of the initially split-up problem together. Furthermore, we extend the algorithm to handle multiple balls, i.e. up to four balls. We start with four balls that are in any periodic orbit, while the paddle trajecotry is as in Section 2.2.1. Most likely all four balls will initially be in the $\mathcal{P}_1^1$-orbit, however, it does not have to. After a certain time, the paddle trajectory is switched

Table 3.2: Overlapping between strange attractor of chaos trajecotry and basin of attraction of stabilizing paddle trajectory - interpolated with WAA

A	$\mathcal{P}_1^3$	${}_{\mathsf{A}}\mathcal{P}_1^2$	${}_{\mathsf{B}}\mathcal{P}_1^2$	$\mathcal{P}_1^1$	$\mathcal{P}_2^1$
0.03	0.0085	0.0996	0.1040	0.3039	0.0046
0.025	0.0050	0.0807	0.0997	0.3866	0.0065
0.02	0.0045	0.0881	0.0957	0.3950	0.0066

Table 3.3: Overlapping between strange attractor of chaos trajecotry and basin of attraction of stabilizing paddle trajectory - interpolated with CA

A	$\mathcal{P}_1^3$	${}_{\mathsf{A}}\mathcal{P}_1^2$	${}_{\mathsf{B}}\mathcal{P}_1^2$	$\mathcal{P}_1^1$	$\mathcal{P}_2^1$
0.03	0.0087	0.1003	0.1047	0.3076	0.0058
0.025	0.0050	0.0811	0.1002	0.3902	0.0078
0.02	0.0046	0.0887	0.0963	0.3994	0.0082

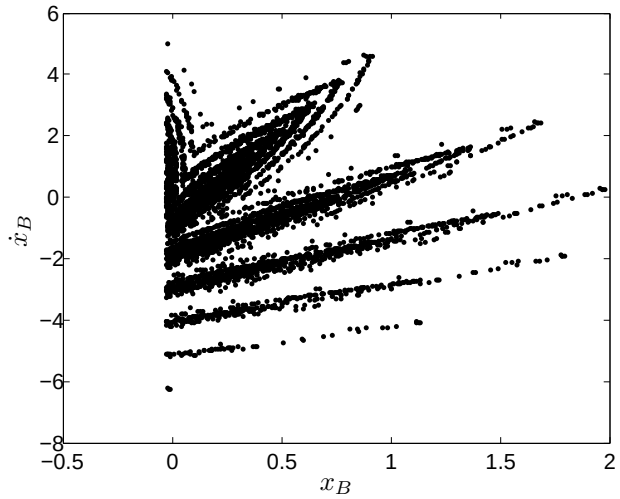

Figure 3.12: Strange attractor for chosen parameters $a_c = 2g$ and $A = 0.03$

into the mode explained in Section 2.2.2. Now, we are looking for a switching time to go back to the stabilizing paddle trajectory such that all desired periodic orbits are reached.

The main part of the algorithm is to find an adequate switching point. The potetial switching points have to be limited to the bottom points of the chaos paddle trajectory, because the basin of attraction was computed for the clearly defined transition part that results if the bottom of the chaos paddle trajectory is chosen as switching point, as it can be seen in Fig. 3.1. The idea is straightforward: While the system is excited with the chaos paddle trajectory, we check at every bottom point of the chaos trajectory whether the paddle trajectory can be switched back to the first mode or not. This is done by testing if the ball's states are part of the desired basins of attraction using an interpolation algorithm. Figure 3.14 shows an example for two balls. An approach to reduce the computation steps will be presented in the next section.

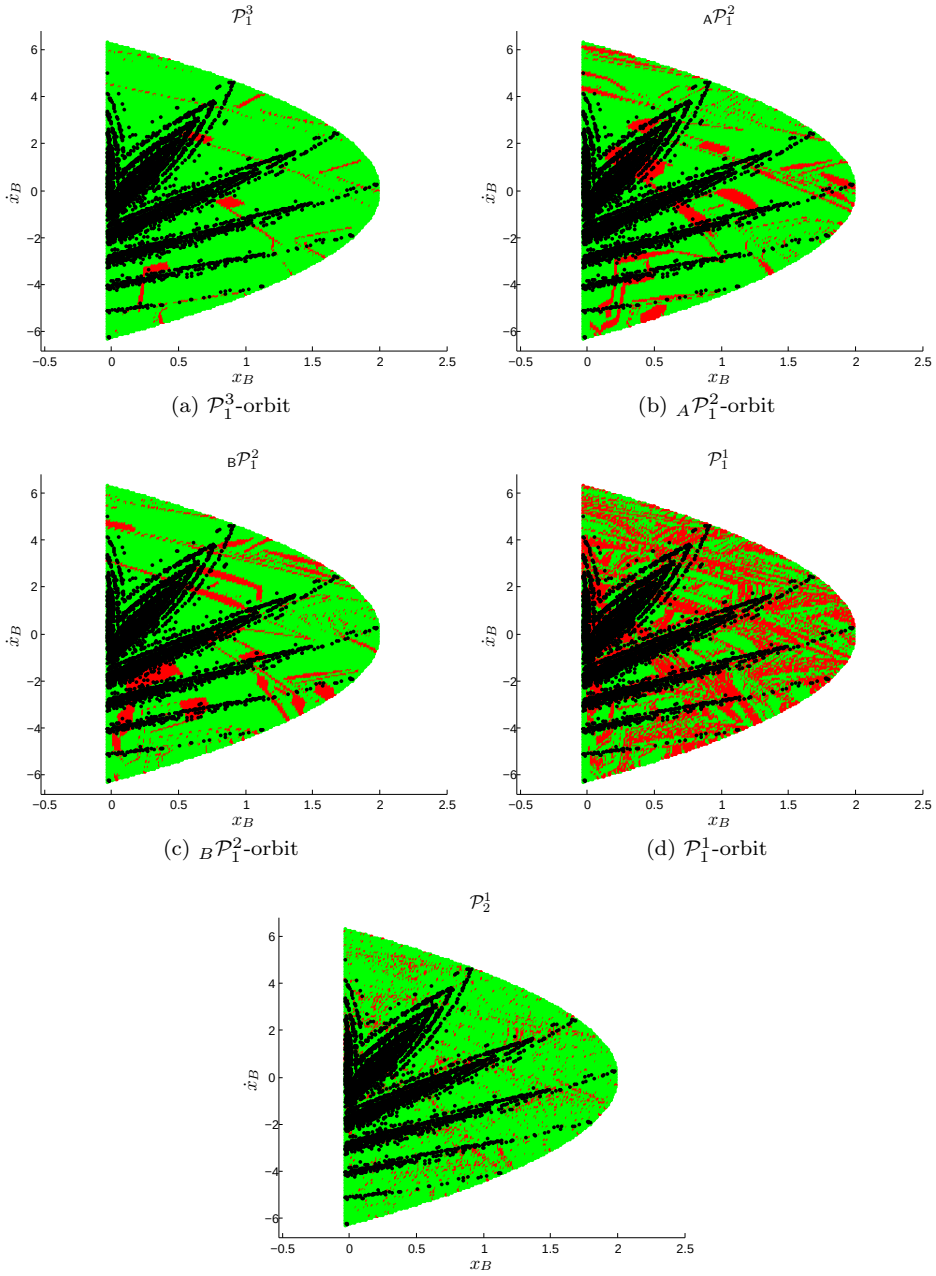

(a) $\mathcal{P}_1^3$-orbit

(b) $_A\mathcal{P}_1^2$-orbit

(c) $_B\mathcal{P}_1^2$-orbit

(d) $\mathcal{P}_1^1$-orbit

(e) $\mathcal{P}_2^1$-orbit

Figure 3.13: Overlapping between strange attractor and basin of attraction

3.4.1 Permutations

For the cloverleaf paddle of the BJR, it would be desirable to reach four different periodic orbits. Because there are 5 feasible periodic orbits, as shown in Section 2.3, we have $\begin{pmatrix} 5 \\ 4 \end{pmatrix} = 5$ different combinations of four different orbits. However, as some periodic orbits have rather small basins of attraction, we can already suppose that it will be hard to reach certain combinations of the orbits in reasonable time. With reasonable time we denote switching times below 5 minutes. Again, a tradeoff between reliability and computation time of the interpolation algorithm

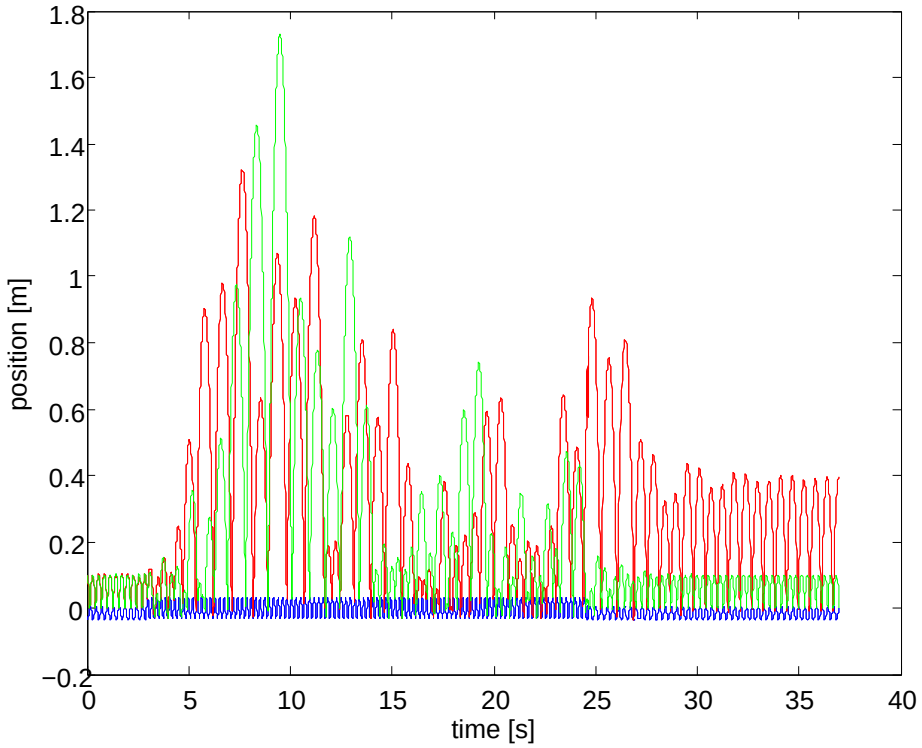

Figure 3.14: Two balls starting in the $\mathcal{P}_1^1$-orbit. After 3 seconds the paddle trajectory is switched and we look for adequate inital conditions of the balls. After 24 seconds the paddle trajecotry is switched back to the stabilizing mode and the desired $\mathcal{P}_1^1$- and ${}_{\mathrm{A}}\mathcal{P}_1^2$-orbit result.

used is required. On the one hand, one could think about applying an interpolation algorithm with low computation time and low reliability. Using that algorithm a trial and error strategy could be pursued, i.e. if the desired periodic orbits do not result after one trial, the paddle trajectory is switched back to the chaos mode and the procedure is repeated until the desired result is achieved. In addition, some learning strategy could be derived to improve the results. On the other hand, an interpolation algorithm could be chosen that does not follow the other, with the goal to reach the desired periodic orbits at the first trial.
To minimize the switching time, we make the assumption that permutations of the balls are not considered. This means that it does not matter which out of the four balls reaches which periodic orbit. However, the total of all four periodic orbits has to match the desired ones. Due to this assumption, one can reduce the number of inital conditions that have to be classified by an interpolation algorithm from 24 to 10, where $4! = 24$ is the number of all permutation $\sigma : \{1, 2, 3, 4\} \to \{1, 2, 3, 4\}$, that a set - containing 4 elements - has. In a sequential consideration of the four balls without permutations, starting with the first ball one has to check its initial conditions at most for four periodic orbits. Going on with the second ball, there are only three orbits remaining that have to be checked in the worst case and so on, which gives ten possibilities. It has to be mentioned that as soon as one ball cannot reach any of the desired periodic orbits, that are checked, we move on to the next switching time.

3.4.2 Approach without using a Basin of Attraction

One could think of an approach similiar to the one presented in this chapter, however, without using a basin of attraction. The main idea is that we know the last impact states of all balls. For the next potential switching point a simulation is executed, to see which periodic orbits would be achieved, if the paddle trajectory was switched to the stabilizing mode. If all desired orbits are reached, the BJR is assigned to switch the paddle trajectory at this specific time. Otherwise, one goes on to the next potential switching point and so on. Without loss of generality, it can be assumed that knowing the last impact state for all balls, no impact of no ball occurs before the potential switching point is achieved, otherwise one would just simple update the last impact state by such an impact. We call this 'shifting window idea'. This approach has the big advantage to not use a basin of attraction and therefore avoid the problems that occur with the interpolation algorithms. The drawback, however, is that potential switching points get lost, because if an impact of a ball occurs just before a potential switching point, the time is not sufficient to execute the simulation described.

While for one ball this approach leads to satisfactory results, for four balls it shows very poor performance because of the drawback explained. Since an algorithm should be derived that can handle four balls, this approach is useless for the given problem setting.

3.5 Evaluation/Discussion

In this section, we discuss the performance of the algorithms presented in this chapter. Several aspects have already been mentioned before, nevertheless they will be repeated to give a well-arranged review of the derived algorithms.

The main advantage of the algorithms presented is, that using an adequate interpolation method each combination out of the five feasible periodic orbits is realized in reasonable time. The main drawback is its low reliability. It is only rarely possible to reach the $\mathcal{P}_2^1$-orbit, due to its fractional basin of attraction, which is plotted in Fig. 3.3(e). The remaining four periodic orbits can be reached with clearly higher reliability. Since the switching times are rather small, one could compensate the low reliability using a trial and error approach, as explained in Section 3.4.1. Another problem is that until now we assumed a noiseless environment and perfect state knowledge which is not realistic for the BJR. Therefore, robustness is another important requirement of the algorithm. One could think of using an interpolation algorithm similar to the RA, with even a larger neighbourhood to increase the robustness, but the drawback of such an approach was already mentioned, when the RA was discussed.
Furthermore, the limitation to the potential switching points of the chaos paddle trajectory, which are each bottom points, is restricting. Of course, further potential switching points, e.g. each top point, could be added by computing new basins of attraction for each new potential switching point. However, even with more potential switching points, there will always be a limited number of possible switching points, which causes high switching times. It would be desirable being able to switch the paddle trajectory at any point using only one look-up table to determine the stability for each periodic orbit.

In Chapter 4, a new approach is presented, with the main goal to get higher ro-

bustness and continuous potential switching points.

Chapter 4

Second Algorithm - Non-Local Stability Analysis

In this chapter, a second approach is presented. The goal is to get rid of the two main drawbacks of the first approach in Chapter 3, namely the low reliability and the limitation to a finite set of potential switching points. The idea is to focus on the stabilizing paddle trajectory for the stability analysis. Unlike in Chapter 3, we only consider the second parabolic piece of the stabilizing paddle trajectory in Fig. 2.3, i.e. the piece where the nominal impact point is located. If we know the region on this trajectory part where the ball with a specific velocity can strike leading to a certain periodic orbit, the transition part between chaos and stabilizing paddle trajectory can be arbitrarily chosen. In other words, a basin of attraction can be computed that is only depending on the stabilizing paddle trajectory and not on some transitional part, as in Chapter 3.

4.1 Local Stability

We want to analyze the stability properties of the fixed points determined by (2.13). Taking advantage of Lyapunov's stability principle, according to [13], the system (2.13) - linearized about an equilibrium point - can be analyzed. We derive a linear mapping that describes how perturbations, added to the initial conditions of the nominal trajectory, map over a single bounce. This approach is motivated by [3] and carried out in the next section, while a nomenclature according to Fig. 4.1 is used.

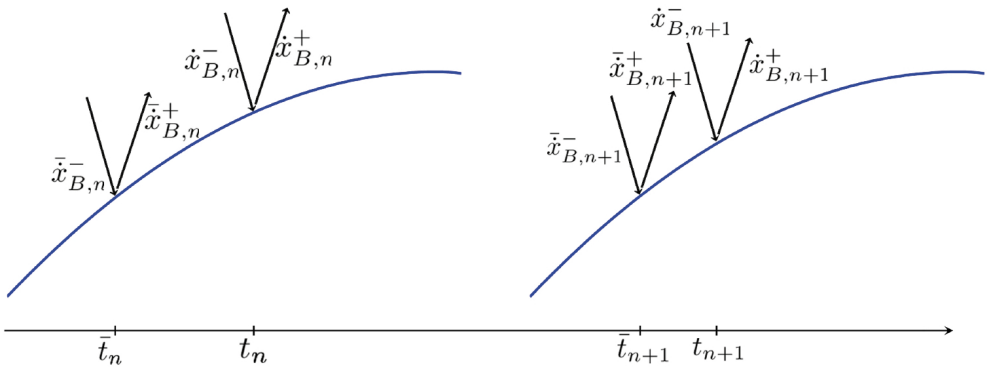

Figure 4.1: Nomenclature for perturbation analysis

4.1.1 Perturbation Analysis

We define the nominal ball and paddle states as

$$\bar{\mathbf{x}}_{\mathbf{B},\mathbf{0}} := \begin{pmatrix} \bar{x}_{B,0} \\ \bar{\dot{x}}_{B,0} \end{pmatrix} = \begin{pmatrix} 0 \\ \bar{\dot{x}}_{B,0} \end{pmatrix} \tag{4.1}$$

and

$$\bar{\mathbf{x}}_{\mathbf{P},\mathbf{0}} := \begin{pmatrix} \bar{x}_{P,0} \\ \bar{\dot{x}}_{P,0} \end{pmatrix} = \begin{pmatrix} 0 \\ \bar{\dot{x}}_{P,0} \end{pmatrix}. \tag{4.2}$$

For the ball state a perturbation is introduced leading to a so-called perturbated state

$$\mathbf{x}_{\mathbf{B},\mathbf{0}} = \bar{\mathbf{x}}_{\mathbf{B},\mathbf{0}} + \sigma_{\mathbf{0}}, \quad \text{with} \quad \sigma_{\mathbf{0}} = \begin{pmatrix} \sigma_{01} \\ \sigma_{02} \end{pmatrix}. \tag{4.3}$$

Now, the dynamics between two impacts can be linearized, where we use at (★), that the impacts of ball and paddle state are assumed to occur instantaneously:

$$\left.\begin{aligned} x_B(\tau) &= 0 + \sigma_{01} + \tau\bar{\dot{x}}_{B,0} \\ x_P(\tau) &= 0 + \tau\bar{\dot{x}}_{P,0} \end{aligned}\right\} \overset{(\bigstar)}{\Rightarrow} x_B(\tau) \overset{!}{=} x_P(\tau) \tag{4.4}$$

Therefore, τ can be computed as

$$\tau = \frac{\sigma_{01}}{\bar{\dot{x}}_{P,0} - \bar{\dot{x}}_{B,0}}. \tag{4.5}$$

To consider how the perturbations map over two impacts, the notation of Fig. 4.1 can be used. The pre-impact state of the ball and paddle at impact n are

$$\mathbf{x}^-_{\mathbf{B},\mathbf{n}} = \begin{pmatrix} \sigma_{01} + \tau\bar{\dot{x}}_{B,0} \\ \sigma_{02} + \bar{\dot{x}}_{B,0} - \tau g \end{pmatrix}. \tag{4.6}$$

and

$$\mathbf{x}_{\mathbf{P},\mathbf{n}} = \begin{pmatrix} \tau\bar{\dot{x}}_{P,0} \\ \bar{\dot{x}}_{P,0} + a_p\tau \end{pmatrix}. \tag{4.7}$$

Using Newton's impact law (2.8), the post-impact state can be computed:

$$\mathbf{x}^+_{\mathbf{B},\mathbf{n}} = \begin{pmatrix} \sigma_{01} + \tau\bar{\dot{x}}_{B,0} \\ -e_z(\sigma_{02} + \bar{\dot{x}}_{B,0} - \tau g) + (1+e_z)(\bar{\dot{x}}_{P,0} + a_p\tau) \end{pmatrix}. \tag{4.8}$$

To describe the free flight phase, we use (2.4), where $2T$ is denoted as one paddle period and we take into account the compensation for τ:

$$\begin{aligned} \mathbf{x}^-_{\mathbf{B},\mathbf{n+1}} &= \begin{pmatrix} -\frac{1}{2}g(2T)^2 + \dot{x}^+_{B,n}2T + x^+_{B,n} - \tau\bar{\dot{x}}_{B,0} \\ -g2T + \dot{x}^+_{B,n} + g\tau \end{pmatrix} \\ &= \begin{pmatrix} -2gT^2 + 2T(-e_z(\sigma_{02} + \bar{\dot{x}}_{B,0} - \tau g) + (1+e_z)(\bar{\dot{x}}_{P,0} + a_p\tau)) + \sigma_{01} + \tau\bar{\dot{x}}_{B,0} - \tau\bar{\dot{x}}_{B,0} \\ -gT + (-e_z(\sigma_{02} + \bar{\dot{x}}_{B,0} - \tau g) + (1+e_z)(\bar{\dot{x}}_{P,0} + a_p\tau)) + g\tau \end{pmatrix} \\ &= \begin{pmatrix} \sigma_{01} + 2T((1+e_z)a_p\tau - e_z(\sigma_{02} - \tau g)) \\ -e_z(\sigma_{02} - \tau g) + (1+e_z)a_p\tau + g\tau \end{pmatrix}. \end{aligned} \tag{4.9}$$

In the last step the relations

$$\bar{\dot{x}}_{P,0} = -\bar{\dot{x}}_{B,0}\frac{1-e_z}{1+e_z} \tag{4.10}$$

and

$$\bar{\dot{x}}_{B,0} = -gT \tag{4.11}$$

were used. Now, the system can be linearized in terms of perturbations. Therefore, with (4.5) and (4.9) we compute the Jacobian

$$\begin{aligned} M := \frac{\partial \mathbf{x}^-_{\mathbf{B,n+1}}}{\partial \boldsymbol{\sigma}_\mathbf{0}} &= \begin{pmatrix} \frac{\partial x^-_{B,n+1}}{\partial \sigma_{01}} & \frac{\partial x^-_{B,n+1}}{\partial \sigma_{02}} \\ \frac{\partial \dot{x}^-_{B,n+1}}{\partial \sigma_{01}} & \frac{\partial \dot{x}^-_{B,n+1}}{\partial \sigma_{02}} \end{pmatrix} \\ &= \begin{pmatrix} 1 + 2T\frac{(1+e_z)a_p + e_z g}{\bar{\dot{x}}_{P,0} - \bar{\dot{x}}_{B,0}} & -2Te_z \\ \frac{e_z g + (1+e_z)a_p + g}{\bar{\dot{x}}_{P,0} - \bar{\dot{x}}_{B,0}} & -e_z \end{pmatrix} \end{aligned} \tag{4.12}$$

From [3] it is known, that the Jacobian M describes the linear mapping of perturbations over the free fall, i.e.

$$\boldsymbol{\sigma}_\mathbf{1} = M\boldsymbol{\sigma}_\mathbf{0}. \tag{4.13}$$

Using $\mathbf{x}^-_{\mathbf{B,n}} = \bar{\mathbf{x}}_{\mathbf{B,0}} + \boldsymbol{\sigma}_\mathbf{0}$ and $\mathbf{x}^-_{\mathbf{B,n+1}} = \bar{\mathbf{x}}_{\mathbf{B,0}} + \boldsymbol{\sigma}_\mathbf{1}$, finally the linearization of the discrete time system, describing the impacts, is obtained as

$$\mathbf{x}^-_{\mathbf{B,n+1}} = M\mathbf{x}^-_{\mathbf{B,n}}. \tag{4.14}$$

For the linear discrete time system (4.14), the conditions for stable equilibrium points are that all eigenvalues of M must lie strictly inside the unit circle, i.e. the absolute value of both eigenvalues has to be smaller than one.

Using (4.10) and (4.11) one gets

$$\bar{\dot{x}}_{P,0} - \bar{\dot{x}}_{B,0} = \frac{2gT}{1+e_z} \tag{4.15}$$

and the characteristic polynomial of M can be derived as

$$\begin{aligned} p_M(\lambda) =& (1 + 2T\frac{(1+e_z)a_p + e_z g}{\bar{\dot{x}}_{P,0} - \bar{\dot{x}}_{B,0}} - \lambda)(-e_z - \lambda) + 2Te_z\frac{e_z g + (1+e_z)a_p + g}{\bar{\dot{x}}_{P,0} - \bar{\dot{x}}_{B,0}} \\ =& \lambda^2 + \lambda\left(e_z - 1 - 2T\frac{(1+e_z)a_p + e_z g}{\bar{\dot{x}}_{P,0} - \bar{\dot{x}}_{B,0}}\right) + \frac{2Te_z g}{\bar{\dot{x}}_{P,0} - \bar{\dot{x}}_{B,0}} - e_z \\ \overset{(4.15)}{=}& \lambda^2 + \lambda\left(e_z - 1 - \frac{1+e_z}{g}((1+e_z)a_p + e_z g)\right) + (1+e_z)e_z - e_z \\ =& \lambda^2 g + \lambda\left((e_z - 1)g - a_p(1+e_z)^2 - (1+e_z)e_z g\right) + e_z^2 g \end{aligned} \tag{4.16}$$

To determine the eigenvalues of M, consider $p_M(\lambda) \overset{!}{=} 0$. Therefore, the following two eigenvalues are obtained:

$$\lambda_{1,2} = \frac{1}{2g}\left(g + a_p(1+e_z)^2 + ge_z^2 \pm \sqrt{(g + a_p(1+e_z)^2 + ge_z^2)^2 - 4e_z^2 g^2}\right) \tag{4.17}$$

It can be seen that the local stability, i.e. the eigenvalues $\lambda_{1,2}$, only depends on the paddle acceleration at impact a_p, the coefficient of restitution e_z and the gravitational constant g. Figure 4.2 shows the maximum absolute eigenvalue for varying paddle accelerations. It can be seen that for the paddle acceleration chosen in Chapter 3, namely $a_p = -\frac{g}{2}$, local stability is guaranteed.

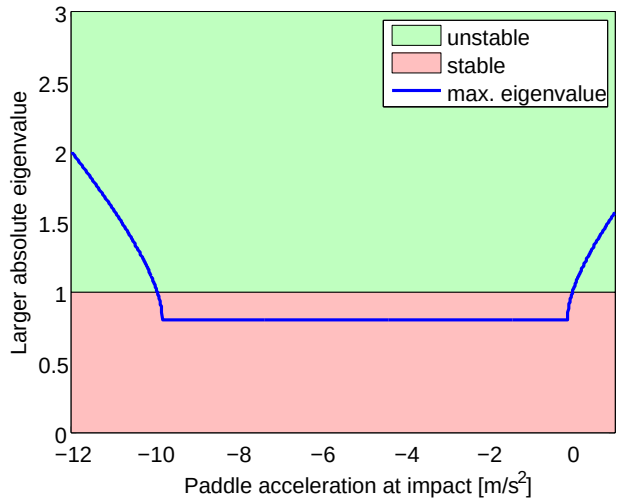

Figure 4.2: Plot of $\max|\lambda_{1,2}|$ for different paddle accelerations at impact a_p

In [5], they now look for an optimal paddle acceleration in the local stable range - here $a_p \in [-10, -0.5]$ - which leads to the largest basin of attraction. However, this will not be done here, since the paddle acceleration $a_p = -\frac{g}{2}$ has been chosen, according to [3], to minimize the H_2 norm over a range of ball properties of the BJR.

4.2 Non-Local Stability

In this section, the basin of attraction starting at the first impact on the stabilizing paddle trajectory is derived. We want to know, where the first impact can occur - with a certain velocity - such that a particular periodic orbit is reached. The derivation is restricted to the $\mathcal{P}_1^1$-orbit. Again, the notation explained in Fig. 4.1 is used. However, some slight changes will be introduced. From (2.13), the mappping

$$\begin{aligned} \mathscr{G}: \quad & \mathbb{R}^2 \to \mathbb{R}^2 \\ & \begin{pmatrix} \dot{x}_{B,n}^- \\ t_n \end{pmatrix} \mapsto \begin{pmatrix} \dot{x}_{B,n+1}^- \\ t_{n+1} \end{pmatrix} \end{aligned} \tag{4.18}$$

is known. We define

$$\tau_n := t_n - \bar{t}_n \tag{4.19}$$

as the perturbation in time and

$$w_n := \frac{1}{g}(\dot{x}_{B,n}^- - \underbrace{\bar{\dot{x}}_{B,n}^-}_{-gT}) \tag{4.20}$$

as a normed velocity perturbation, in order to have the same units and scaling of both states. This scaling will later be useful to define a numerical criterion for convergence. It has to be mentioned, that $\bar{\dot{x}}_{B,n}^-$ is determined by the particular periodic orbit, e.g. for the $\mathcal{P}_1^1$ orbit, $\bar{\dot{x}}_{B,n}^-$ is equal to $-gT$. Other periodic orbits could be analyzed by adjusting this value. Using the two normed states, the following

mapping is obtained:

$$\begin{aligned} \tilde{\mathscr{G}}: \quad & \mathbb{R}^2 \to \mathbb{R}^2 \\ & \begin{pmatrix} w_n \\ \tau_n \end{pmatrix} \mapsto \begin{pmatrix} w_{n+1} \\ \tau_{n+1} \end{pmatrix}. \end{aligned} \tag{4.21}$$

Because only one parabolic piece of the paddle trajectory from Section 2.2.1 is considered, there is a physical bound for τ:

$$\tau \in [\tau_{\min}, \tau_{\max}]. \tag{4.22}$$

In this chapter we denote with initial condition the ball state at the first impact. To compute the basin of attraction we want to know, which initial conditions converge to the nominal point $\bar{\mathbf{x}} = \begin{pmatrix} \bar{\tau} \\ \bar{w} \end{pmatrix} = \begin{pmatrix} 0 \\ 0 \end{pmatrix}$. We denote an initial condition as converged to the nominal state after i iteration steps, if

$$|\tau_i| + |w_i| < \epsilon \quad \text{and} \quad |\tau_j| + |w_j| \geq \epsilon, \quad \forall j < i, \quad i, j \in \mathbb{N}_0. \tag{4.23}$$

Since we want to achieve high robustness, the initial conditions should converge in a reasonable number of iteration steps.

To compute the basin of attraction, an initial condition is chosen and using the mapping (4.21), the states are iterated. Therefore, the system (2.13) has to be solved, which is done by a numerical solve routine. During all iteration steps, the bound (4.22) has to hold, otherwise the initial condition is classified as unstable. Figure 4.3 shows the basin of attraction with different maximum iteration steps allowed to converge. Of course, the explicit number of iteration steps is depending on the factor ϵ, which is used to define numerical convergence, i.e. for a bigger value of ϵ less iteration steps may be needed to converge. Since the same value for ϵ is used for all simulations, Fig. 4.3 shows how the basin of attraction grows considering more iteration steps. It can also be seen that the basin of attraction is limited, i.e. in spite of the allowed iteration number is increased from 50 to 100 steps, the basin of attraction does not change anymore. It should be reminded that the analysis in this chapter simply focuses on the $\mathcal{P}_1^1$-orbit.

The ideas presented in this chapter, specificly for the $\mathcal{P}_1^1$-orbit, can be easily extended to the other periodic orbits. Knowing the basins of attraction for all periodic orbits, the same interpolation algorithms could be used. However, at least for the $\mathcal{P}_1^1$-orbit, the basin of attraction is one connected domain, so the interpolation should be much more reliable than in Chapter 3. The aspect of robustness, i.e. assuming that the ball states are not exactly measured, can be taken into consideration by reducing the basin of attraction as shown in Fig. 4.3(e) such that even if the real states vary slightly from the measured ones, they still lie inside the basin of attraction.

As mentioned, one main advantage of this new approach is that the basin of attraction is only depending on the stabilizing paddle trajectory. Therefore, the switching point on the chaos paddle trajecotry and an appropriate transition part can be arbitrarily chosen. This dramatically increases the number of potential switching points and at first sight it should lead to a much faster performance compared with the approach in Chapter 3. The main drawback is that with this approach the strange attractor, describing the initial conditions realized with the chaos paddle trajectory

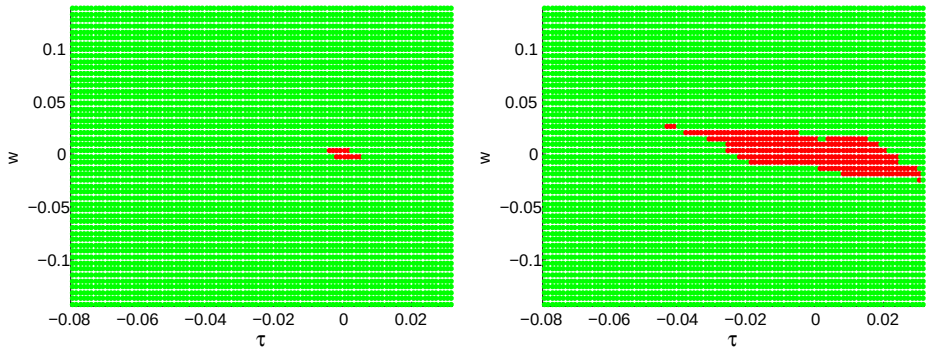

(a) Max. 10 iteration steps

(b) Max. 20 iteration steps

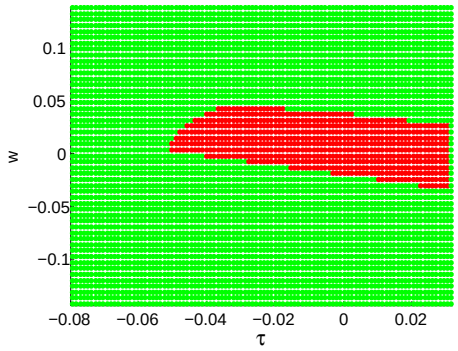

(c) Max. 50 iteration steps

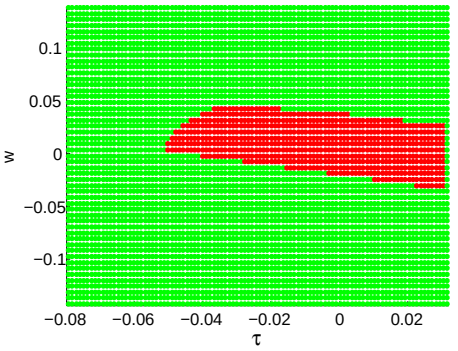

(d) Max. 100 iteration steps

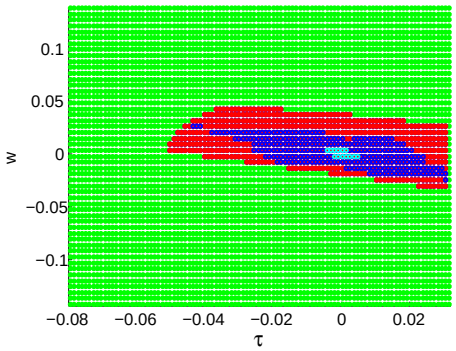

(e) Comparison of the 4 basins of attraction

Figure 4.3: Basin of attraction

depends on the transitional part. For each arbitrarily chosen switching point a new transition trajectory is introduced and there is no guarantee, that the strange attractor really overlaps with the particular basin of attraction. Another problem, having an infinite number of potential swiching points, is the realtime implementation. Since time is needed to measure states and verify them using the precomputed basin of attraction, the potential switching points have to be limited to such points that are realizable in realtime. However, using a sophisticated method to implement this algorithm the problem should be highly reduced. Last but not least, since the basin of attraction for the $\mathcal{P}_1^3$-, ${}_A\mathcal{P}_1^2$-, ${}_B\mathcal{P}_1^2$- and $\mathcal{P}_2^1$-orbit have not been computed, the performance of the two approaches from Chapter 3 and 4 can only be compared for the $\mathcal{P}_1^1$-orbit. However, for this single orbit, the approach from Chapter 4 is preferred.

Chapter 5

Conclusion and Future Work

The main contribution of this thesis is the following: A strategy has been developed and numerically verified that can realize an arbitrarily chosen combination out of the five feasible periodic orbits, for up to four balls juggling at the same time. One main part to derive the algortihm was the determination of the basin of attraction for each periodic orbit, which was performed numerically by gridding the set of all physically feasible initial conditions. As this is done with a finite resolution, several interpolation methods have been derived to classify initial conditions. We discovered that especially the $\mathcal{P}_2^1$-orbit is highly sensitive, since its basin of attraction is fragmented, i.e. it contains no large connected domain. Furthermore, it turned out that an interpolation algorithm should be favored, which focuses on large connected domains in the basin of attraction, since the reliability is increased doing so. Unfortunatelly, for the $\mathcal{P}_2^1$-orbit, no such large domain exists which leads to the decision to either approve a lower reliability or eliminate it as a feasible periodic orbit.

In a further investigation, a paddle trajectory was designed to excitate the balls, such that they enter the basin of attraction of the desired periodic orbits. Therefore, aperiodic long term behaviour of the system is highly desired to reach different regions at the state space. Additionally, a sensitivity on initial conditions is needed to 'break the symmetries', as explained in (3.3). This two requirements lead to the decision of choosing the paddle's motion in such a fashion that chaotic motion is obtained.

Further research might focus on the approach initiated in Chapter 4, which possibly will lead to a better robustness since the basins of attraction only in the neighbouhood of the nominal initial condition are considered. Furthermore, it would be challenging to analytically compute the basin of attraction, which should be possible for the mentioned approach, since only one quadratic polynomial part of the paddle trajectory is considered. This could be done similar to [7], by finding a Lyapunov function that proves stability, even if finding an appropriate Lyapunov function is a highly demanding task.

A topic which probably is worth thinking about in more depth, would be to add noise to the simulation. Therefore, the ball's state and the coefficient of restitution could be corrupted by noise. Last but not least, having a control strategy that is reliable in the presence of noise, it would be interesting to implement it to the BJR.

List of Figures

List of Tables

Bibliography

[1] Tyler Abbott Nicholas B. Tuffilaro and Jeremiah Reilly. *An Experimental Approach to Nonlinear Dynamics and Chaos*. Addison-Wesley Publishing Company, 1992.

[2] Andrew R. Teel Ricardo G. Sanfelice and Rodolphe Sepulchre. A hybrid systems approach to trajectory tracking control for juggling systems. *test journal*, 2007.

[3] Philipp Reist and Raffaello D'Andrea. Bouncing ball in three dimensions with a blind jugging robot. *Proceedings of the 2009 IEEE international conference on Robotics and Automation, Kobe, Japan*, 2009.

[4] D.E Koditschek M.Bühler and P.J. Kindlmann. A simple juggling robot: Theory and experimentation. *Proceedings of the First International Symposium on Experimental Robotics*, 1990.

[5] Dagmar Sternad Stefan Schaal and Christopher G. Atkeson. One-hand juggling: A dynamical approach to a rhythmic movement task. *Journal of Motor Behaviour*, 1995.

[6] Thomas L. Vincent. Controlling a ball to bounce at fixed height. *Proceedings of the American Control Conference, Seattle, Washington*, 1995.

[7] Thomas Heimsch and Remco Leine. Lyapunov stability theory for non-smooth non-autonomous mechanical systems applied to the bouncing ball problem. Center of Mechanics, ETH Zurich, 2008. Master Thesis.

[8] Renaud Ronsse. Rhythmic movements control: Parallels between human behavior and robotics. Université de Liège. Doctoral Thesis.

[9] Philipp Reist Matthias Fässler and Raffaello D'Andrea. Estimation of ball coefficient of restitution for the blind juggler, 2010. Semester Thesis.

[10] Steven H. Strogatz. *Nonlinear Dynamics and Chaos*. Westview Press, 1994.

[11] Angelika Steger. *Diskrete Strukturen*. Springer-Verlag Berlin Heidelberg, 2001.

[12] Gerd Fischer. *Lineare Algebra*. Vieweg and Teubner, 1975.

[13] Lino Guzzella. *Analysis and Synthesis of Single-Input Single-Output Control Systems*. vdf, 2009.

ETH
Eidgenössische Technische Hochschule Zürich
Swiss Federal Institute of Technology Zurich

Institut für Dynamische Systeme und Regelungstechnik
Prof. Dr. R. D'Andrea, Prof. Dr. L. Guzzella

Title of work:

A Dynamical Approach to Create Different Juggling Patterns Using Chaos

Thesis type and date:

Bachelor Thesis, June 2010

Supervision:

Philipp Reist
Prof. Dr. Raffaello D'Andrea

Student:

Name:	Tobias Sutter
E-mail:	suttert@student.ethz.ch
Legi-Nr.:	07-908-122
Semester:	6

Statement regarding plagiarism:

By signing this statement, I affirm that I have read the information notice on plagiarism, independently produced this paper, and adhered to the general practice of source citation in this subject-area.

Information notice on plagiarism:

`http://www.ethz.ch/students/semester/plagiarism_s_en.pdf`

Zurich, 20. 7. 2010: _____